Tutorial

Photophysical Properties of Anthracene Derivatives

Agonist Kastrati, Franck Oswald, Antoine Scalabre and Katharina M. Fromm *

Department of Chemistry, University of Fribourg, Chemin du Musée 9, CH-1700 Fribourg, Switzerland; franck.oswald@unifr.ch (F.O.)
* Correspondence: katharina.fromm@unifr.ch

Abstract: In this tutorial review, we intend to provide the reader with a comprehensive introduction to the photophysical properties of organic compounds with a specific focus on anthracene and its derivatives. Anthracene-based building blocks have attracted the attention of chemists due to their intrinsic luminescent properties. A deep understanding of their interaction with light, including the mechanisms of emission (luminescence, i.e., fluorescence or phosphorescence) and quenching, is crucial to design and generate compounds with precise properties for further applications. Thus, the photophysical properties of different types of aggregates, both in the ground state (J- and H-type) and in the exited state (e.g., excimer, exciplex) will be discussed, finishing with a few examples of dyads and triads.

Keywords: anthracene; light; spectra; electron; photopysics; emission

1. Introduction

1.1. Light

Light is based on electromagnetic waves having defined wavelength and frequency. [1] The electromagnetic wave (just as the name states) is composed of electric and magnetic oscillation fields that are perpendicular to each other (Figure 1).
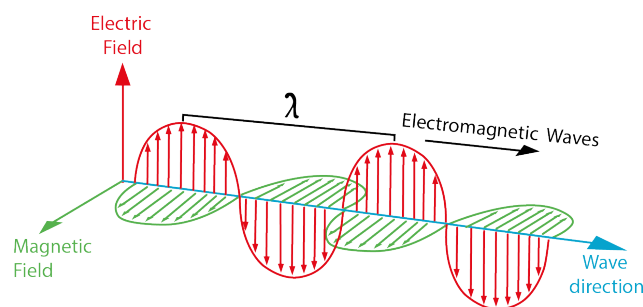

Figure 1. Electric and magnetic properties of polarized light shown on behalf of linearly polarized light at a given time point.

All types of light (e.g., gamma, UV, visible, IR) have the same nature, but what differentiates them is their wavelength and frequency. Some of them are higher energy and shorter wavelengths (e.g., gamma rays), while others are lower energy and possess longer wavelengths (e.g., infrared). The energy of light is inversely proportional to its wavelength: if the wavelength increases, the energy decreases and vice versa (Equation (1)).

$$E = \frac{hc}{\lambda} \tag{1}$$

E = energy of light, h = Planck's constant 6.625×10^{-34} Js, c = speed of light 2.998×10^8 m/s, λ = wavelength.

Undisputedly, light is one of the most important phenomena for all living species on earth, mainly because it provides the energy needed for living species to function. Thus, green plants use sunlight to synthesize sugars via the process of photosynthesis (Figure 2), while the produced sugars in turn are used by living organisms.
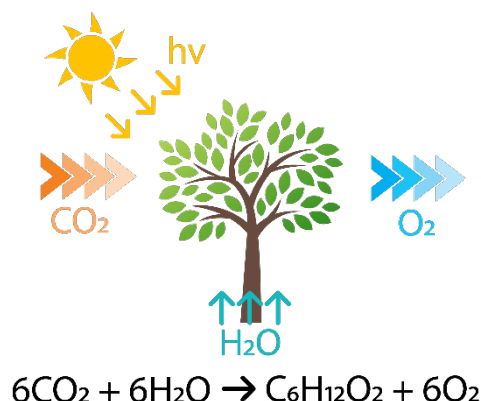
$$6CO_2 + 6H_2O \rightarrow C_6H_{12}O_2 + 6O_2$$

Figure 2. Photosynthesis reaction.

Photosynthesis, apart from producing carbohydrates, further helps balance the amount of carbon dioxide and oxygen as it uses the carbon dioxide (respiratory byproduct of living organisms) to release oxygen. The reaction is possible thanks to the chlorophyll found in green plants, capable of harvesting the light and converting it into chemical energy (carbohydrate) while transforming carbon dioxide in the presence of water to carbohydrates (sugar) and oxygen [2].

Another important feature of light is that it helps living beings to see and differentiate between objects due to their different absorptions, a topic that is going to be explained in more detail below. The main source of light for many years was the Sun, giving a wide range of radiation (herein wavelength λ nm), which can also be used to perform photochemical reactions as stated by Ciamician in 1912 [3]. While the human eye is able to detect only a small part of the entire spectral range, mainly from 380 to 780 nm, the rest of the radiation requires special techniques for its detection (Figure 3).
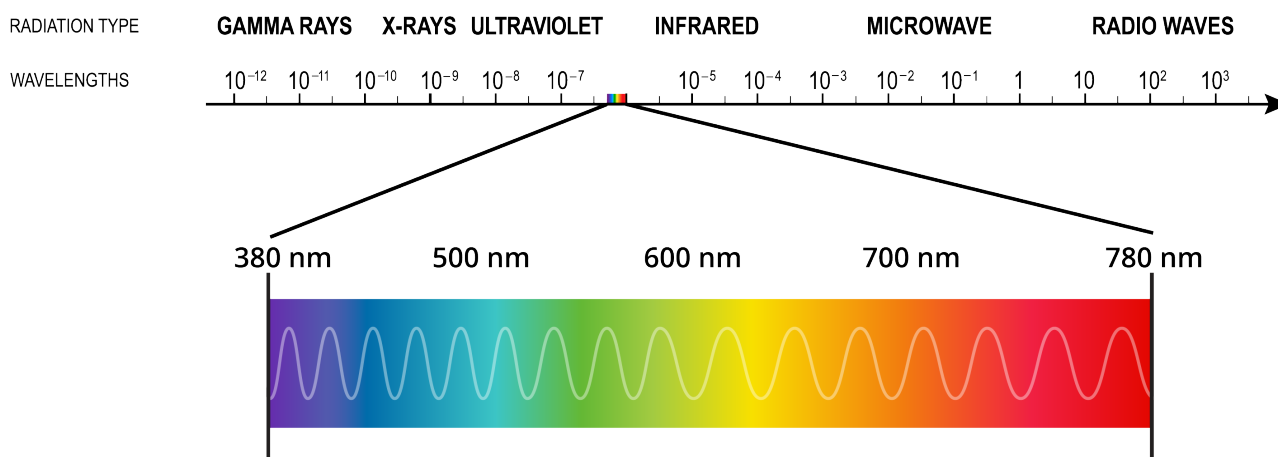
Figure 3. Region of light in the electromagnetic spectrum with a zoom on the visible region.

Light Sources

We can differentiate two types of light sources: natural (created by nature, animals) and artificial (created by humans). Some of them are listed below (Figure 4).
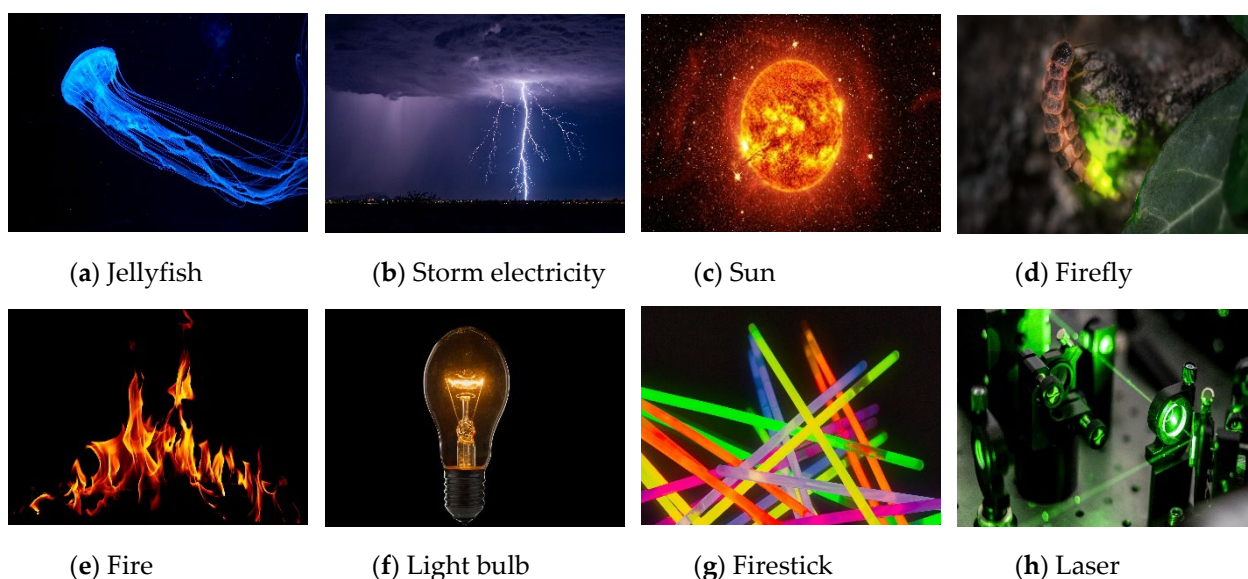
(**a**) Jellyfish   (**b**) Storm electricity   (**c**) Sun   (**d**) Firefly

(**e**) Fire   (**f**) Light bulb   (**g**) Firestick   (**h**) Laser

Figure 4. Light source picture: natural above, artificial below.

1.2. Interaction of Light with Matter

1.2.1. Absorption

Absorbance, also known as *optical density*, refers to the light absorbed by matter, whether it is gas, liquid, or sold. The absorbance corresponds to the logarithm of the ratio between the intensity of light before entering the matter (solid, gas, liquid) (I_0) and the intensity of light after passing through that medium (I_s) (Equation (2)).

$$A = Iog \ \frac{I_0}{I_s} \tag{2}$$

However, there are other physical processes that can contribute to minimizing the light intensity while light is passing through a specific medium, such as reflection or scattering. Thus, the measurement of the outgoing light intensity does not only show the absorbance, but it measures the attenuation caused by all these processes together. Different chromophores have different capabilities of absorbing light. The capability of absorbing light by a chromophore material is known as its extinction coefficient (ε), and it can easily be determined through the Lambert-Beer law by measuring the absorbance (A) of a solution of the compound with a known concentration (c) in a cell with a known width (l) (Equation (3)).

$$A = \varepsilon \cdot l \cdot c \tag{3}$$

1.2.2. Matter

Matter is any material (gas, liquid, solid) that takes up space (volume) and has mass. It is composed of atoms as the smallest constituent. While matter is composed of atoms, the latter is composed of protons, neutrons, and electrons. Protons are positively charged, influencing the electronic configuration of the atoms, and define the atomic number. Neutrons, on the other hand, do not affect the electronic configuration because they are chargeless. However, atoms that differ in neutron number are called isotopes, e.g., carbon has three naturally occurring isotopes, ^{12}C, ^{13}C, and ^{14}C. In the first case, the carbon atom has six protons and six neutrons given a total mass number of 12 ($^{12}_{6}C$); in the second case, it has six protons and seven neutrons given a mass number of 13 ($^{13}_{6}C$) whereas in the latter case, it has eight neutrons and six protons given a mass number of 14 ($^{14}_{6}C$). Contrary to positively charged protons, electrons are negatively charged, being responsible for numerous physical phenomena, such as: magnetism (since it has a spin), electricity (because

it is a charge species), and chemistry (responsible for bond formation, thus influencing physical and chemical properties). The space around the nucleus where an electron is found with high probability is often called the orbital (Figure 5).
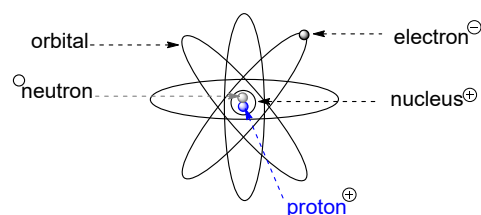

Figure 5. Atomic structure.

When two atoms come close in proximity under proper condition (right orbital geometry, temperature, pressure, etc.), their orbitals will overlap (by sharing their electrons) with each other to form a new molecule. The newly formed molecules, on the other hand, have two new molecular orbitals: the highest occupied molecular orbital (HOMO) bonding, fully occupied, and the lowest unoccupied molecular orbital (LUMO) antibonding and empty orbitals. Such an example is the formation of a π-π bonding by the overlap of two π orbitals of two carbon atoms (Figure 6).
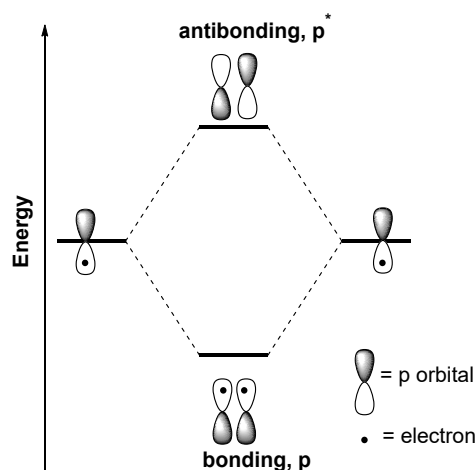

Figure 6. π orbitals in a typical π bonding (bonding and antibonding *).

1.2.3. Electronic Transitions

Electronic transitions happen when matter absorbs or emits light. We already learned that the atom is the smallest constituent of matter and that it possesses at least one electron in its atomic orbitals. Thus, in principle, everything can interact with light. Excitation of such compounds with a proper wavelength will cause an electron transition from the ground state (bonding orbital) to the excited state (antibonding orbital). Depending on the type of light and the chemical composition, all possible electronic transitions that typically can occur when a compound absorbs light are depicted in (Figure 7).
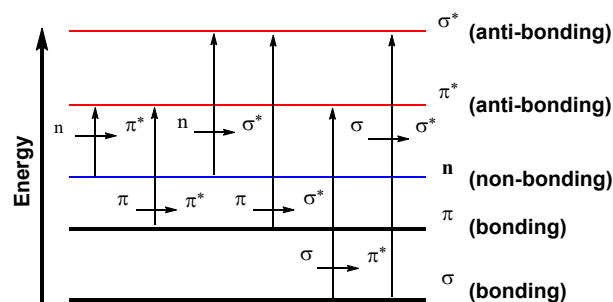
Figure 7. Most common electronic transitions (n, π, σ).

Singlet and triplet excited states are commonly used terms to describe these (processes) transitions as they are more informative. In the singlet excited state (antibonding orbital), the electron is still antiparallel after excitation, whereas in the tripled excited state, the electron is parallel due to the spin flip (Figure 8).
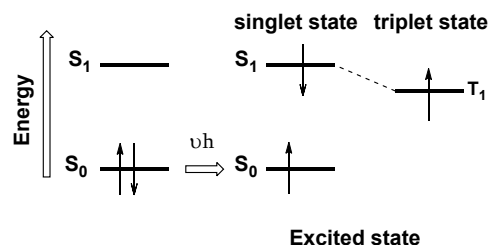

Figure 8. Singlet and triplet excited state.

Electron transition from HOMO to LUMO can be promoted by providing energy that matches the exact energy difference between the ground state and the final state (Figure 8). Typical electronic transitions are these involving n, π, σ, d-d, and ligand-to-metal or metal-to-ligand charge transfer transition (LMCT, MLCT). However, traditional benchtop UV–VIS spectrometers with wavelengths of 200–800 nm can only observe n-π*, π-π*, d-d, and charge transfer electronic transitions. This is because the wavelength that is provided by these analytical techniques is not sufficient to promote σ-σ* electronic transitions, which require a lot more energy to lift an electron from the ground state to the exited state (Figure 7). The n-π* transition occurs in the compounds containing hetero atoms, e.g., amines or carbonyl compounds, which contain nonbonding electrons. Because the energy gap between these two different energy states is promoted compared with the other ones, e.g., sigma (σ), the energy required to trigger this transition is rather low. Therefore, in a typical UV absorption spectrum, the absorption band appears at higher wavelength. The π-π* transition, on the other hand, is found in compounds containing double (carbonyl groups, double bonds) or triple bonds, and because the energy gap between these two states is larger than for n-π*, the UV absorption band appears at lower wavelength. Such transitions are observed in the case of benzophenone, which contains both types of electrons, thanks to the carbonyl functional group (Figure 9).
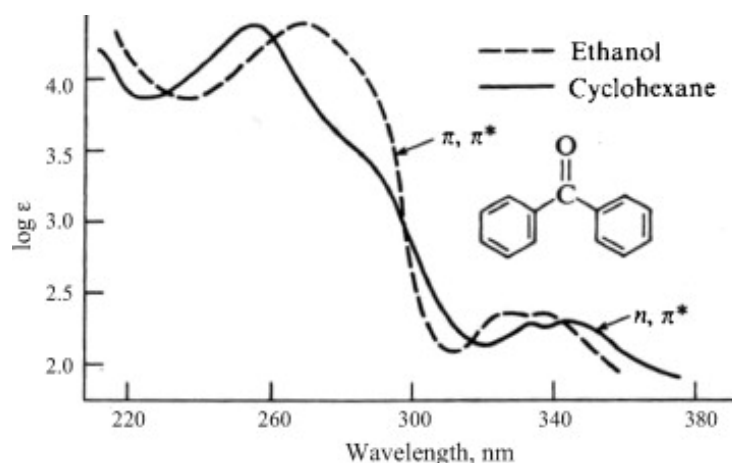
Figure 9. Absorption spectrum of benzophenone in ethanol (dotted line) and in cyclohexane (solid line) Reprinted adapted with permission from Ref. [4]. Copyright 2008, Elsevier.

However, this is not true for all compounds because conjugation capabilities between different compounds containing double bonds lead to different absorption bands. Such an example is depicted in Figure 10. As the conjugation increases from naphthalene to anthracene and tetracene, the absorbance spectrum shifts to higher wavelength, with tetracene absorbing at around λ = 400–500 nm. This is caused mainly because in tetracene, there are four phenyl rings fully conjugated. Thus, tetracene is a colored compound with a characteristic number of absorption bands (four).

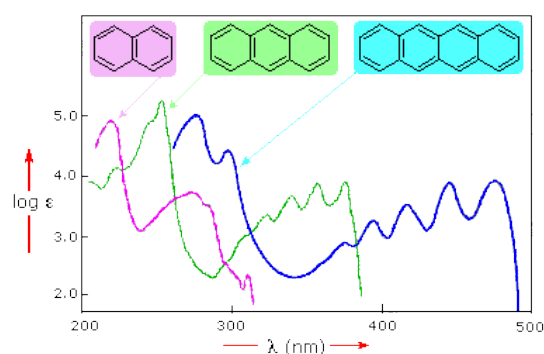**Figure 10.** UV–VIS absorption spectrum of different conjugated systems "Adapted with permission from [5,6], Copyright 2023, Jones, R.N.".

In contrast to the first two examples, the energy gap between σ-σ* is large as it involves compounds having only sp³ C–H; thus this excitation requires wavelengths in the far UV region, and this type of transition usually is not observed in UV–VIS [7], as shown for cyclohexane (Figure 11).
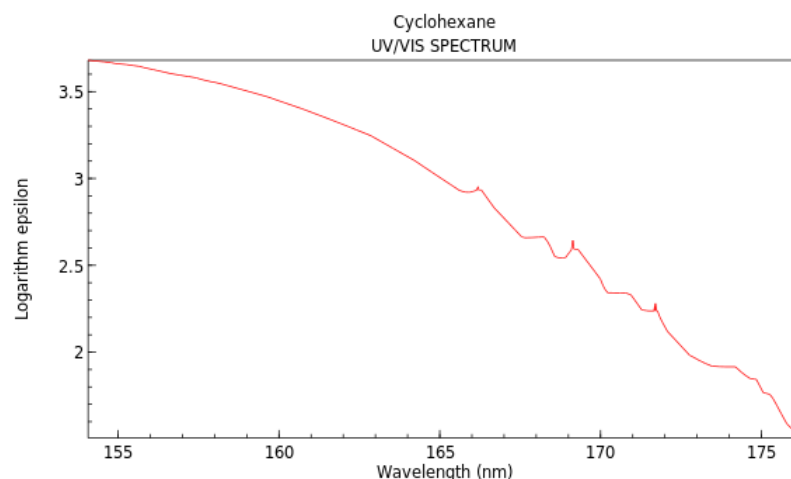
Figure 11. UV–VIS spectrum of cyclohexan. "Reprinted with permission from Ref. [8]. Copyright 2019, Elsevier"

Charge transfer (CT) and d-d transitions are usually found in inorganic compounds since they typically contain metal ions, which, in combination with ligands, sometimes allow such transition to occur [9]. The d-d transition usually is observed from transition metal ions' complexes when one electron from a lower d orbital energy state is promoted and jumps to another d orbital of higher energy state; however, this transition is forbidden by the Laporte rule [10]. This rule is mainly applied for those compounds that possess centrosymmetric point symmetry. It states that all transitions that conserve parity during the electronic transition either going from p-p or d-d are forbidden, but s-p and p-d are allowed. However, if the centrosymmetry is disturbed, the Laporte rule can be overcome, and the transition can take place (Figure 12).
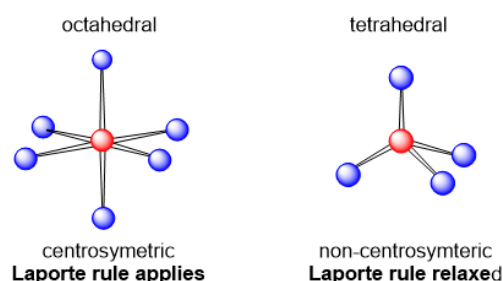

Figure 12. Geometry influence in Laporte selection rule.

While in the d-d transition, an electron transfer from a lower energy *d* orbital occurs to another d-orbital of higher energy, in the case of charge transfer in either MLCT or LMCT, the electron transition occurs from the metal to the ligand and vice versa, where one of them is capable of donating electrons and the other one is capable of accepting that electron. Such examples are usually met in the case of metal–ligand complexes.

All transition necessitates the absorption of a photon in a first step, and the resulting excited compound (very reactive species) can afterward experience a photochemical reaction, leading to a new product, or can go back to the ground state via fluorescence or phosphorescence emission. However, there are some restrictions during these processes because some of these transitions are allowed while others are not, according to the selection rules: any transition that implies that the reaction entropy is not zero ($\Delta S \neq 0$) is strongly forbidden. A typical example is the absorption of a photon from a chromophore, which indeed leads almost always to the formation of the singlet excited state (allowed transition) and not the triplet excited state (forbidden transition). This is because, in the first case, the transition occurs between states of the same multiplicity ($S_0 + \nu h \rightarrow S_1$),

whereas in the latter, it occurs with a different multiplicity ($S_0 + vh \rightarrow T_1$), which otherwise would involve change in the spin state (Figure 13).
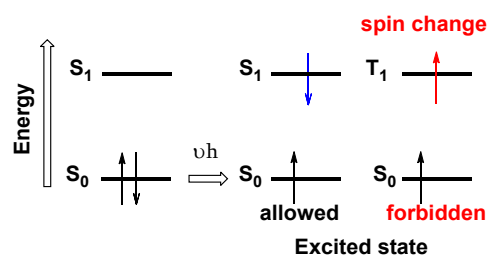

Figure 13. Spin selection rule $\Delta S = 0$.

1.2.4. Emission

Jablonski Diagram

All photochemical processes including photochemical reactions, fluorescence, phosphorescence, and other processes related can be represented in a Jablonski diagram as shown in Figure 14. For any of these phenomena to occur, a photon having the exact energy needed to transfer an electron from the ground state to the excited state must be absorbed.
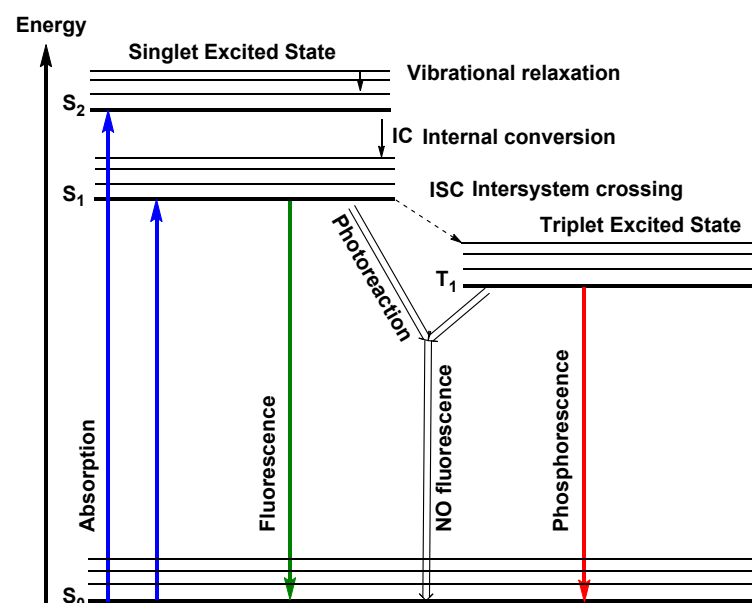

Figure 14. Jablonski diagram.

ΔE is the energy difference between the two states, v is the frequency of the photon absorbed, h is Planck's constant (6.62×10^{-34} J s), and λ is the wavelength (Equation (4)).

$$\Delta E = hv, \ v = \frac{c}{\lambda} \tag{4}$$

The absorption of the photon can provoke a change in the electronic distribution of matter, thus changing the reactivity and therefore leading to either a photochemical reaction, fluorescence, or phosphorescence emission. According to Kasha's rule, fluorescence always occurs from the lowest singlet excited state (S_1). However, excitation usually takes place to higher energy levels than S_1 (e.g., S_2, $S_3 \ldots S_n$). In addition, each excited state usually is associated with the access of vibrational energy (v) (e.g., v = 0, 1, 2…n), which relaxes quickly (time scale 10^{-13} to 10^{-9} s in the condensed phase) to v = 0 as heat. It can also undergo fast internal conversion (IC) S_2–S_1, within 10^{-9} to 10^{-7} s. From this point, it can go

back to the ground state in four possible ways: (a) via a chemical reaction giving new products, (b) by emission of the absorbed photon (fluorescence), (c) by intersystem crossing (ISC) through the change of spin to reach the triplet excited state (T_1), and (d) by internal conversion (IC) by heat emission, which further can lead to photochemical reaction or phosphorescence (Figure 14) [11]. Fluorescence and phosphorescence phenomena will be explained below in more detail.

Fluorescence

The fluorescence process, as depicted in the Jablonski diagram (Figure 15), consists in the absorption of a photon with minimum energy by a chromophore [12] to bring an electron to an excited state. The emission of light (photon) then occurs from the lowest singlet excited state. The emitting light has thus a longer wavelength and therefore lower energy than the absorbed wavelength because some of its energy is lost during the processes of vibrational relaxation and internal conversion, which in turn are much faster than the fluorescent emission (Figure 15).
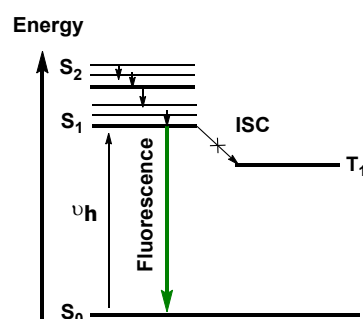

Figure 15. Simplified Jablonski diagram for fluorescence.

One of the most appealing examples of fluorescence is when the absorption process occurs in the UV, invisible region for the human eye, and emits in the visible region. Since its discovery, fluorescence, due to its intrinsic properties and easy detection, has been used to detect optical properties and found widespread applications in light-emitting diodes (LEDs) [13–15], chemical sensors [16–18] for toxic compounds [19–22], nitro derivatives, herbicides [23–29], and medicine [30–34].

Quenching Mechanism

Quenching of fluorescence is the decrease of the fluorescence intensity as a function of the fluorophore's (donor) interaction from either the ground or the excited state, with

its surroundings, e.g., the solvent or a specific quencher molecule (good quenching properties are complex formation through hydrogen bonds (donor/acceptor), π-π interactions, high reduction potentials). For instance, the heavy atom effect [35,36] (spin–orbit coupling, where the electron spin is affected due to the orbital motion of electrons and the electrostatic field of the positively charged nucleus; therefore, the heavier the atom is, the more electrons there are and thus the more the electron spin is affected) is a well-known process for fluorescence quenching [37] due to the facilitation of intersystem crossing. The Jablonski diagram (Figure 14) explains all possible phenomena that can occur after the process of light absorption from a chromophore to generate the excited state from which the emission can occur, from either the singlet excited state or the triplet state. Thus, the emission of fluorescence in principle can be quenched either from the ground state by forming a complex with another molecule, which would modify its photophysical properties, or from the excited state by performing a photochemical reaction, or via energy transfer, e.g., via (FRET) Förster resonance energy transfer and (DET) Dexter energy transfer, and via collision. However, all these possible quenching processes can be grouped into dynamic and static quenching.

Dynamic quenching occurs when an excited molecule (donor) collides or is in proximity to an acceptor molecule, and hence, electron transfer becomes possible. It was Förster [38] in 1951 who proposed the electron transfer mechanism as one of the possible ways of quenching (Scheme 1, left). According to him, due to charge oscillations, the donor and acceptor can be affected if they are in close proximity (~10 nm) in order to transfer one electron from the single excited state of the donor to an excited state, which has to be lower in energy, of the acceptor (Scheme 1). However, for this process to occur, there should be an overlap between the emission of the donor and the absorption of the acceptor molecule.
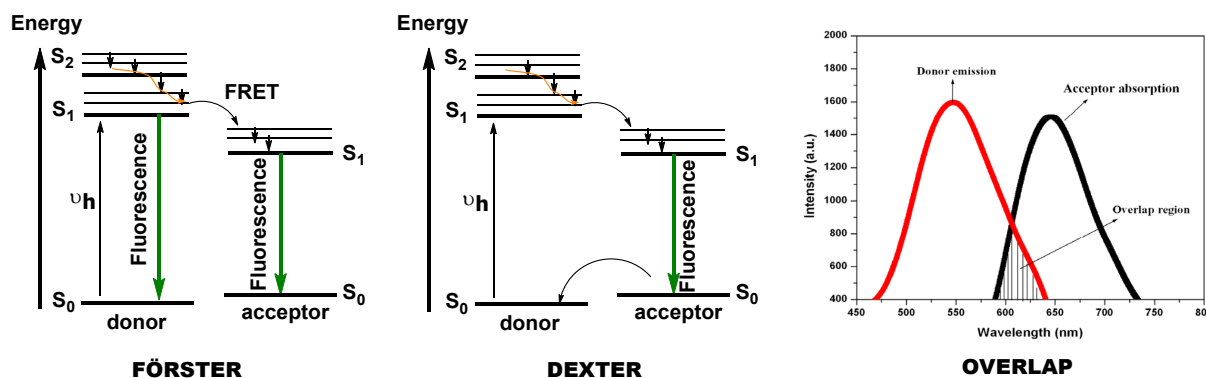
Scheme 1. Quenching mechanism of fluorescence using a Jablonski diagram. Forster (**left**) [39], Dexter (**middle**), and the right overlap between the emission and absorption (**right**) "Adapted with permission from Ref [40], Copyright 2011, Elsevier".

Two years later in 1953, Dexter [41] proposed another mechanism for luminescence quenching. The quenching process can occur when the donor and the acceptor are at a ca. 10 Å distance from each other, sufficient for an overlap of their orbitals. This will automatically lead to an electron transfer from the excited state of the donor to the LUMO of the acceptor, and at the same time, an electron moves from the HOMO of the acceptor to the HOMO of the donor (Scheme 1, center). Participation of excimers (see page 21) in the quenching mechanism was discussed by Weller (1969) [42], and Watkins (1974) a few years later [43].

In contrast to dynamic quenching, static quenching occurs when the fluorophore and the quencher form a complex [44] via π-π interaction, hydrogen bonding, or a chemical reaction in the ground state, therefore changing the photophysical properties of the fluorescent fluorophore to nonfluorescent. Such a process is also observed in the formation of dimers, such as in the case of pure anthracene (see photodimerization in Section 1.3.1).

Both static and dynamic quenching processes depend on the temperature, but follow different laws, allowing us to distinguish between them. Thus, dynamic quenching increases as the temperature increases. This is obvious since the process is based on the collisions between molecules, and the higher the temperature, the more intermolecular interactions. In static quenching, the quenching decreases as the temperature increases since the quencher and fluorophore are poorly bound to each other, and this interaction is weakened as the solution is heated. In addition, during the static quenching, the fluorescence lifetime remains the same (compared with unquenched system) because the quenching process occurs in the ground state, not in the excited state.

1.2.5. Stern–Volmer Relationship

Intermolecular quenching of luminescence (fluorescence/phosphorescence in the presence of another molecule, here called quencher, Q) is a well-known process. In addition, it is known that the quenching process, depending on the type of fluorophore and the quencher, can be static or dynamic. Therefore, whether it is one or the other taking

place in a particular system, it can be easily found out by using the Stern–Volmer relationship [45] (Equation (5)).

$$\frac{F_0}{F} = 1 + K_q\,\tau_0 \cdot [Q] \; , \qquad \frac{F_0}{F} = 1 + K_s \cdot [Q] \tag{5}$$

F_0 is the fluorescence intensity in the absence of the quencher, F is the fluorescent intensity in the presence of the quencher, Q is the quencher concentration, τ is the lifetime of fluorescence in the presence of the quencher, τ_0 is the lifetime in the absence of the quencher, K_q is the quenching rate coefficient, and K_s is the association constant.

The Stern–Volmer relationship allows for investigating intermolecular deactivation by exploring the kinetic of deactivation. Since the static and dynamic quenching act with different mechanisms and thus different kinetic, the Stern–Volmer relationship allows for studying and differentiating between the two. This process can be represented as simplified in (Equation (6)),

$$M^* + Q \rightarrow M + Q \qquad \text{or} \qquad M^* + Q \rightarrow M + Q^* \tag{6}$$
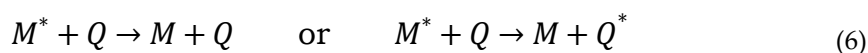
with M being the ground state fluorophore, M^* the excited fluorophore, Q the quencher, and Q^* the excited quencher. Intermolecular quenching in the dynamic mode diminishes both the emission intensity and the lifetime of the fluorescent species. Therefore, the terms $\frac{F_0}{F}$ and $\frac{\tau_0}{\tau}$ against the concentration of the quencher follow the same trend (Figure 16a). However, with static quenching, because of the quencher and the fluorophore complex in the ground state, the number of potential fluorescent species decreases, thus only decreasing the emission intensity without changing the lifetime of the emission; hence the term $\frac{\tau_0}{\tau}$ is independent of the concentration of the quencher.
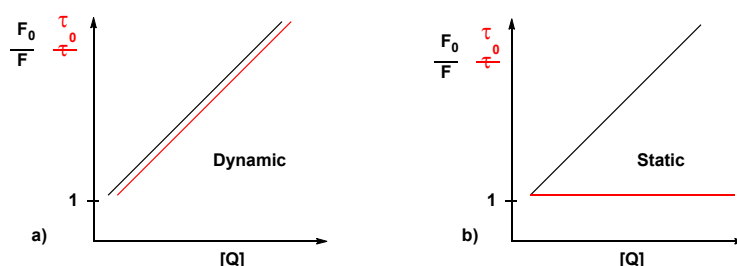

Figure 16. Stern–Volmer graph for dynamic (**a**) and static (**b**) quenching.

Phosphorescence

Phosphorescence is another type of photoluminescence process, consisting in the absorption of light by a chromophore like for fluorescence, but it differs from the latter in its emission process: in fluorescence, emission occurs from the lowest singlet excited state, whereas in phosphorescence, emission occurs from the lowest triplet excited state (Figure 17).
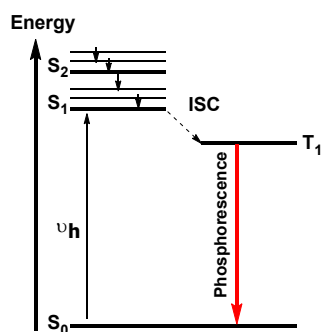

Figure 17. Simplified Jablonski diagram for phosphorescence.

Due to the spin forbidden nature of the emission process, the emission itself is much slower during phosphorescence and can proceed within minutes or up to a few hours [46,47]. An example of long-lasting phosphorescence emission (up to few hours) based on strontium aluminate materials (SrAl$_2$O$_4$:Eu:Dy) was reported by the group of Zitoun, Bernaud, et al. [48] in 2009.

1.3. Anthracene and Its Derivatives

Anthracene is one of the simplest polycyclic aromatic hydrocarbon compounds derived from coal tar (1.5% anthracenes) as the main source. Anthracene belongs to the family of polycyclic aromatic hydrocarbons (PAHs), a class of organic compounds containing multiple aromatic rings [49]. It is composed of three fused benzene rings and is an example of an organic compound acting as a metal-free triplet photosensitizer. A photosensitizer, on the other hand, is a chemical entity capable of harvesting light (energy) and transferring it to its surroundings (molecules), which otherwise could not absorb at this wavelength. This class of organic compounds is particularly attractive for dye-sensitized solar cells [50,51], semiconductors, OLED [52], or lasers [53]. The heavy-metal-free triplet photosensitizer properties of anthracene lie in the fact that the energy levels of the singlet excited state (S$_1$) and of the triplet excited state (T$_2$) are in close proximity (Scheme 2, left), allowing for efficient (up to 70%) intersystem crossing (ISC) [54,55]. However, substitution of anthracene **1** in positions 9 and 10 with phenyl groups as in **2** (diphenylanthracene) [56] prevents π-π stacking and inhibits intersystem crossing simply due to noncoplanar phenyl groups to the anthracene moiety, which ultimately leads to a difference in the singlet and tripled excited states, resulting in a preferred fluorescence rather than phosphorescence emission (Scheme 2, right) [57]. In addition to the favorable energy (small) difference between (S$_1$) and (T$_1$) on anthracene moiety, the close proximity effect during the π-π stacking is another factor that favors ISC, suppressing one of the two preventing it.
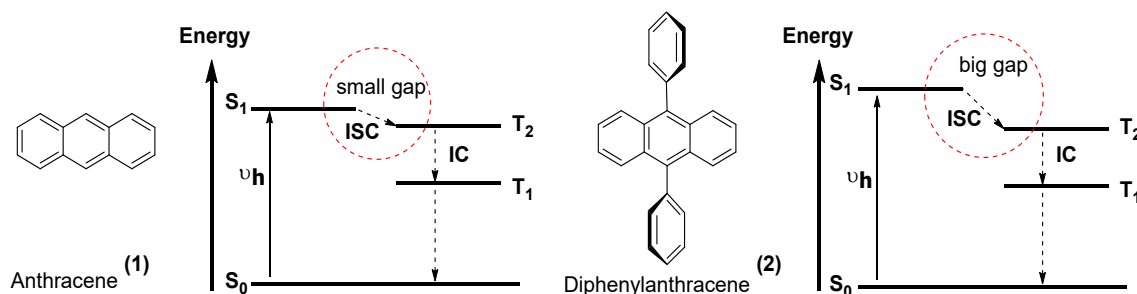
Scheme 2. Mechanism of intersystem crossing, anthracene (**left**), and diphenylanthracene (**right**) "Adapted with permission from Ref. [57]. Copyright 2021, American Chemical Society".

Due to its rigid, planar, electron-rich, and fully conjugated structure, the anthracene compound is known to react via: (i) Diels–Alder [4 + 4] and [4 + 2] cycloadditions, forming the dimer **3** and the peroxide **6** [58], in the presence of another anthracene molecule or singlet oxygen, respectively; (ii) electrophilic substitution to obtain **4** [59], and (iii) oxidation [60] to the anthraquinone **5** (Scheme 3).
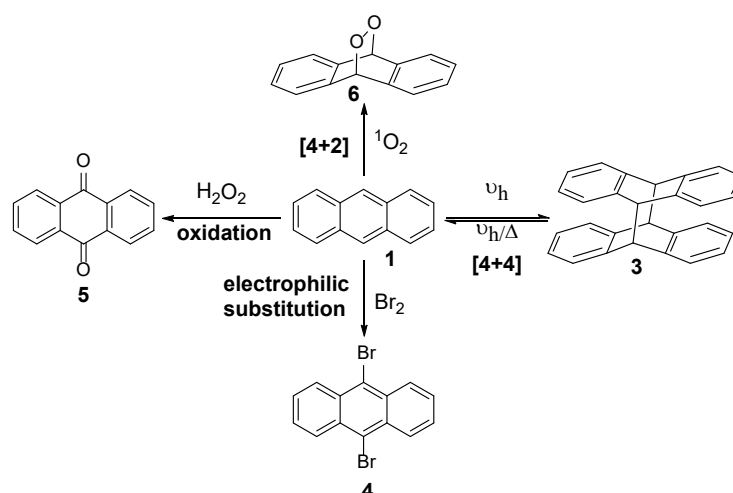
Scheme 3. Anthracene reactions; [4 + 4] (photodimerization), [4 + 2] cycloaddition, electrophilic substitution, and oxidation in positions 9, 10.

Such very diverse reactions of anthracene are of high importance in chemistry. The electrophilic substitution allows the synthesis of many different derivatives (e.g., halides, **4**), which can further be used as precursors for synthesis of desired anthracene derivatives using cross-coupling reactions (e.g., Suzuki cross coupling). Of the same importance is the oxidation to the anthraquinone **5**, where the two carbonyl groups would allow for further functionalizing the anthracene core simply by nucleophilic addition, followed by reductive aromatization [61,62]. Bulky substituted anthracene derivatives suppress inter- and intramolecular interactions due to steric hindrance, consequently enhancing the fluorescence emission. Nevertheless, they can still react with compounds reasonably small, such as with singlet oxygen to generate nonfluorescent endoperoxide compounds **8** as possible oxygen storages [63] (Scheme 4) [64].
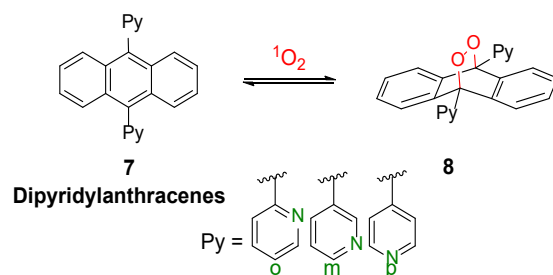
Scheme 4. Oxygenation of dipyridylanthracenes and reconversion of the aromatic endoperoxides (EPOs "Adapted with permission from Ref. [64]. Copyright 2017, American Chemical Society".

The reaction of anthracene derivatives with singlet oxygen is of high importance as oxygen is very abundant in air and solubilized in almost all solvents. Thus, when using anthracene-based sensors, for sensing, one needs to work in oxygen-free solvents to avoid misleading results.

1.3.1. Photodimerization

The photochemical dimerization of anthracene and its derivatives upon exposure to UV light is known since 1867 when Fritzsche isolated the dimer product of anthracene irradiated in benzene solution [65].

Dimerization of anthracene and its derivatives occurs via [4 + 4] photocycloaddition reaction, otherwise thermally forbidden due to the symmetry rules. The reaction involves absorption of a photon from the anthracene monomer in the ground state (S_0), bringing it to the singlet (S_1) or triplet (T_1) excited state. The excitation induces a change in the HOMO

orbital symmetry of the excited anthracene monomer, which is like the LUMO orbital symmetry of the other anthracene monomer in the ground state, allowing them to form an exciplex (excited complex of two species), which then ultimately leads to the formation of the dimer **3** (out of several possible isomers) due to the formation of four benzene rings (and hence the thermodynamically more stable state). Subjecting **3** to thermal conditions leads to quantitative formation of the anthracene **1** (retro Diels–Alder reaction), possibly taking advantage of the strained bridge bonds (Figure 18). Furthermore, the reduced conjugation system in the dimer (ortho-disubstituted benzene) makes it absorb much less light than anthracene (Figure 19).
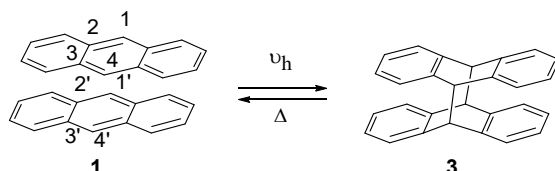

Figure 18. Anthracene photodimerization "Adapted with permission from Ref. [65]. Copyright 1867, Verlag GmbH & Co. KGaA, Weinheim".
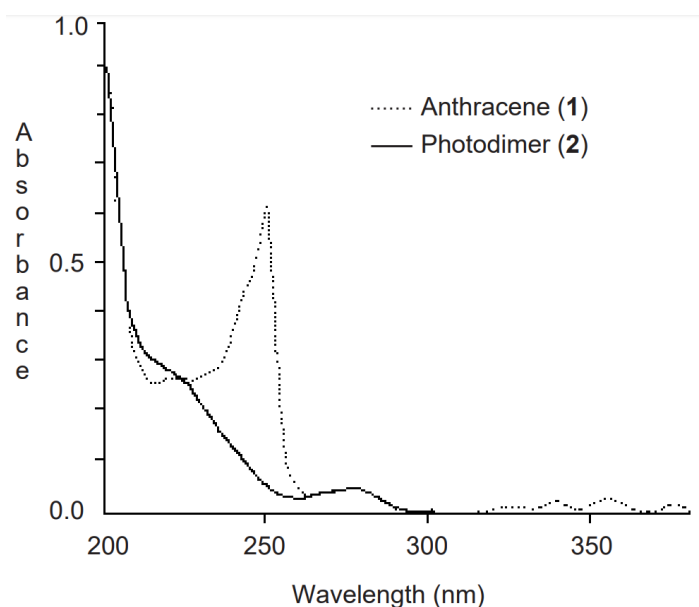

Figure 19. Comparative UV spectra of **1** (4×10^{-6} M) and **3** (5×10^{-5} M) as solutions in CH_3CN "Reprinted with permission from Ref. [66]. Copyright 1955, American Chemical Society".

Over the years, many publications have been reported on the dimerization of anthracene derivatives bearing different substitutions in different positions. To give further chemical evidence for such dimerization reaction of anthracene, Greene et al. in 1955 reported the synthesis of 9-substituted (**9a–9c**) anthracene derivatives with different functional groups (formyl, carbomethoxy, hydroxymethyl) (Figure 20) [67].
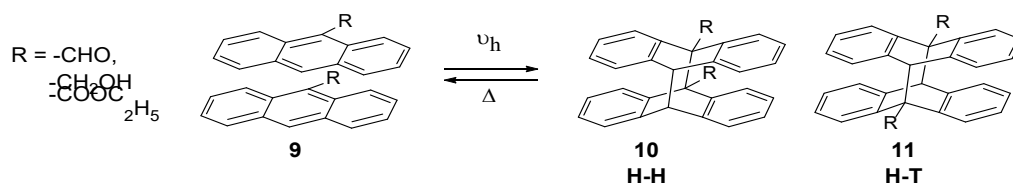

Figure 20. Photodimerization of anthracene "Adapted with permission from Ref. [67]. Copyright 2019, Wiley-VCH Verlag GmbH & Co. KGaA".

During their work, it was found that the solvents (benzene, chloroform, acetic acid, and ethanol) did not influence the rate of dimerization, which was roughly equal. However, the presence of different substituents in position 9 considerably increased the rate of dimerization, with the rate increasing going from 9-methoxycarbonyl (-CHO, **a**), 9-formyl (-CH$_2$OH, **b**), and 9-carboethoxy (-COOC$_2$H$_5$, **c**) proceeding smoothly.

Mechanism of Photodimerization

The mechanism of photodimerization has been extensively studied both in solution [67–70] and in the crystalline form [71]. Greene et al. observed that the ease of the dimerization reaction was roughly the same for several organic solvents. Furthermore, the product isolated was found to be the head-to-head photodimerization product (Figure 20), clear evidence that the reaction proceeds via a radical process **12** and not through a pericyclic intermediate **13** as an alternative mechanism (Figure 21).
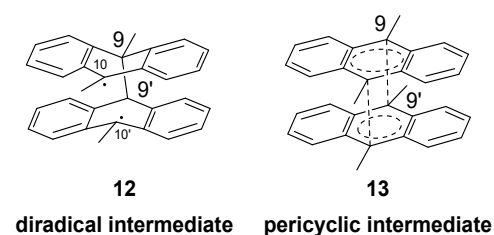

12   **13**

diradical intermediate   **pericyclic intermediate**

Figure 21. (**Left**), diradical intermediate, no bonding between 10 and 10' position; (**right**), pericyclic intermediate, partial bonding between meso position [69].

Reactions proceeding in a concerted manner through a cyclic geometry transition state are known as pericyclic reactions. Those involving a diradical intermediate are reactions where in the first step a radical formation is induced by light and then the resulting diradicals can cyclize after combination to form the photochemical product. In case of an ionic mechanism, one would expect to obtain the head-to-tail products **11** through intermediate **14** (Figure 22).

9   **14**   **11**

R = CHO   **H-T**
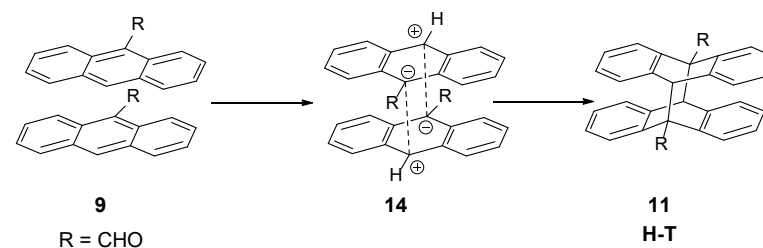
Figure 22. Possible ionic mechanism of anthracene dimerization "Adapted with permission from Ref. [67]. Copyright 1955, American Chemical Society".

1.3.2. Photophysical Properties

Due to these versatile reactions and the intrinsic fluorescent properties, anthracene-based compounds have attracted many researchers to synthesize and design different derivatives to modify and improve their photophysical properties. In this chapter, we will briefly discuss the photophysical properties of different anthracene derivatives.

We commence by discussing some interesting mechanofluorochromic properties of anthracene derivatives **15a–15b** reported by Kusukawa et al. [72] (Scheme 5).

15a: R = CF$_3$
15b: R = CN

1,8-diphenylanthrace derivatives

(15a-15b)
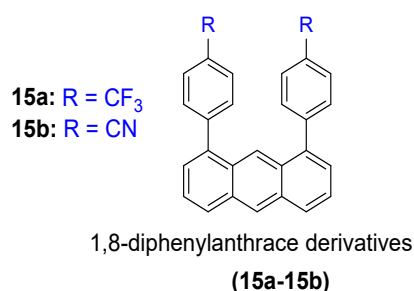
Scheme 5. Chemical structure of 1,8-diphenylanthracenes.

Compounds that change their emission properties upon mechanical stress, e.g., grinding and pressing, are known as mechanochromic.

Fluorophores capable of responding to mechanical stress, such as grinding or pressing, are interesting candidates for applications in sensors [73] and memory chips [74]. This response is caused mainly by the change in the conformation, π-π stacking, and degree of conjugation with a possible mechanism depicted in Scheme 6.
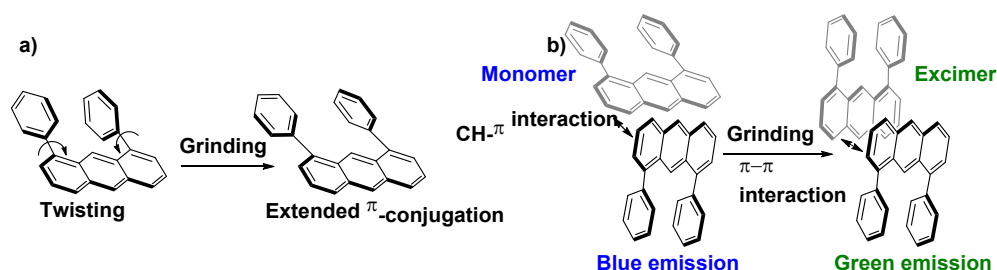
Scheme 6. Possible mechanism for the mechanofluorochromism of the 1,8-diphenylanthracene derivatives, (**a**) twisting of phenyl groups, and (**b**) excimer formation after grinding. "Reprinted permission from Ref. [72]. Copyright 2021, Elsevier B.V".

The changes caused after grinding are clearly observed in the emission spectrum in the case of compounds **15a** and **15b** bearing different substituents. In addition, in the first case, **15a,** a partial self-recovery to a bluish emission, is observed (Figure 23a,b).
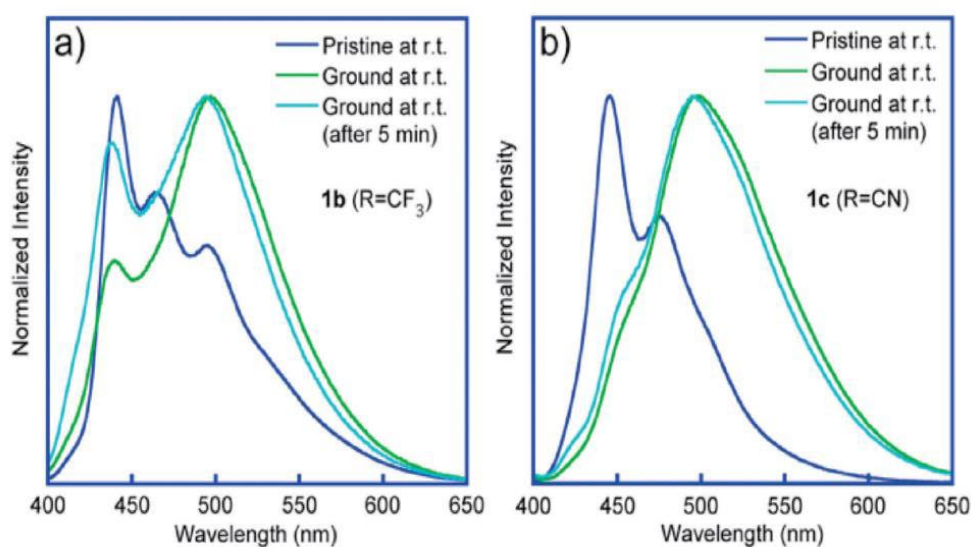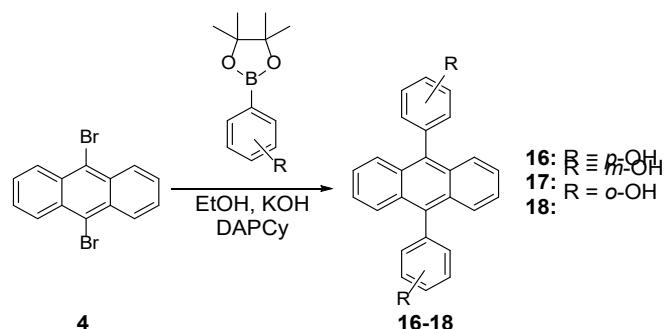

Figure 23. Fluorescence spectra of different states excited at 365 nm, (**a**) **1b** (R = CF$_3$), (**b**) **1c** (R = CN) Reprinted permission from Ref. [72]. Copyright 2021, Elsevier B.V.

In 2007, the group of Slugovc et al. [75] reported the influence of the hydroxy groups in the photophysical properties under the neutral and alkaline condition using *ortho*, *meta*, and *para* isomers of **16**, **17**, and **18** (Scheme 7).

Scheme 7. Synthesis of 9,10-bis(p-hydroxyphenyl)anthracene.

Under neutral conditions, the ligand was fully protonated, and all three derivatives (**16–18**) showed a well-structured absorption spectrum like simple anthracene. In the deprotonated form at basic pH, the absorption spectrum was red-shifted and slightly broadened. While, for the absorption, no major change was observed between the three derivatives under different pH conditions (neutral, basic), a striking result was observed in the emission. A drastic decrease in intensity from a quantum yield of 80% in the protonated form at neutral pH to only 1% in basic pH was observed for compound **17**, which is attributed to drastic change of the electronic properties in the excited state (Figure 24).
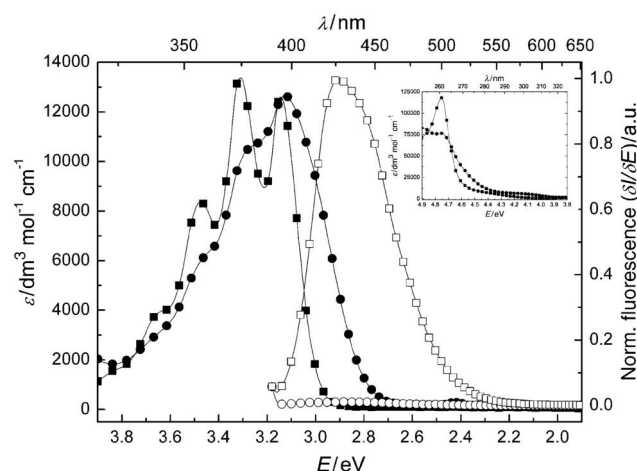
Figure 24. Absorption and emission spectra of **16** in MeOH. ■ Absorption of the protonated species, ● absorption upon addition of NaOH, □ emission of the protonated species (λ_{exc} = 375 nm), and ○ emission upon addition of NaOH. Reprinted with permission from Ref. [75]. Copyright 2007, Springer-Verlag".

Another series of anthracene-based derivatives, this time with an alkyne moiety incorporated, was reported by the group of Wei et al. [76] in 2017 (Scheme 8).

19   **20**   **21**
19a: R = OMe, 19b: R = CHO   20a, 21a: R = H 20b, 21b: R = OMe
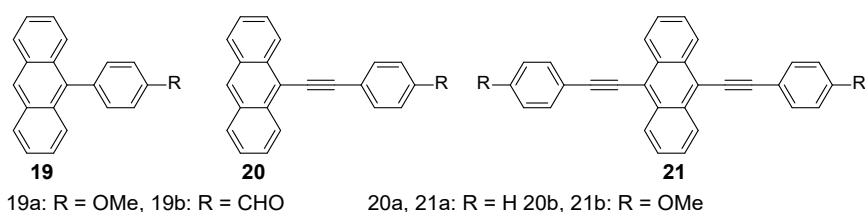
Scheme 8. Anthracene derivatives **19**, **20**, and **21**.

Just as expected, different substituents strongly affected their photophysical properties.

Both absorption and the emission spectra for all three derivatives were investigated in dichloromethane as solvent. Going from compound **19** to **21**, a red shift in the absorbance is observed where the well-structured absorption spectrum in **19** is dissipated into two broader peaks in **20**, which are even more obvious in **21**. The bathochromic shift is mainly due to the increase in the conjugation system by adding either phenyl, which increases the π system to some extent, or a coupled phenyl alkyne system, which increases it even more, confirming once again the influence of different types of substituents [77] in the absorption and emission properties (Figure 25A). The same difference is observed in the emission spectrum where all derivatives emit in the region of blue to bluish green. A more prominent difference in emission is found between compounds **19a** and **19b**, where, in addition, the large Stokes shift (113 nm) in compound **19b** reveals the difference between the electronic ground and excited states of this compound, apparently due to the aldehyde electron withdrawing group, which expands the conjugation system, therefore lowering the HOMO–LUMO gap (Figure 25B). Photophysical properties for these compounds are summarized in Table 1.
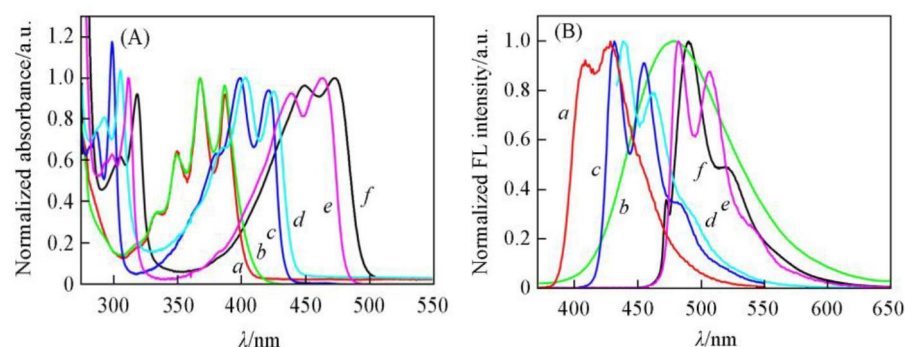

Figure 25. Normalized UV–VIS absorption(**A**) and FL(**B**) spectra of compounds **19**, **20**, and **21** recorded in dichloromethane at about 10^{-5}–10^{-6} mol/L and 25 °C, a. 19a; b. 19b; c. 20 a; d. 20b; e. 21a; f. 21b Reprinted/ with permission from Ref. [76]. Copyright 2017, The Editorial Department of Chemical Research in Chinese Universities and Springer-Verlag GmbH.

Table 1. Photophysical properties of compounds **19**, **20**, and **21**.

Compd.	λ_{max}^{abs} [a]/nm	λ_{max}^{PL} [a]/nm	Stokes Shift [a]/nm	F_f [b]	$\frac{\tau}{ns}$ [b]
19a	349, 367, 387	407, 428	61	0.41	4.59
19b	349, 367, 387	480	113	0.20	3.10
20a	399, 421	431, 455	32	0.54	4.77
20b	404, 424	438, 461	34	0.75	4.26
21a	438, 463	482, 506	19	0.59	3.57
21b	449, 472	490	18	0.57	2.61

[a] Maximum absorption wavelength measured in dichloromethane at about 10^{-5}–10^{-6} mol/L and 25 °C; [b] the quantum yields were measured in dichloromethane using quinine sulfate in sulfuric acid (Φ = 0.55) as the standard.

Other π-extended anthracene fluorophores (**22**) and (**23**) (Figure 26) were synthesized by the group of Wang et al. [78] involving a π-π conjugation system in the lateral direction and n-π conjugation in the longitudinal direction through the nitrogen atom, which establishes a π-n-π conjugation (the nitrogen lone pair serves as a bridge to connect the two aromatic systems). Both compounds showed strong luminescent emission in solution and in the solid state with face-to-face (π-π) interactions dominating the arrangement, whereas the C/N-H…π interactions observed in the lattice of compound **23** probably are

due to the presence of the trimethylsilyl (TMS) groups, posing steric hindrance for face-to-face interaction, thus avoiding possible excimer formation.
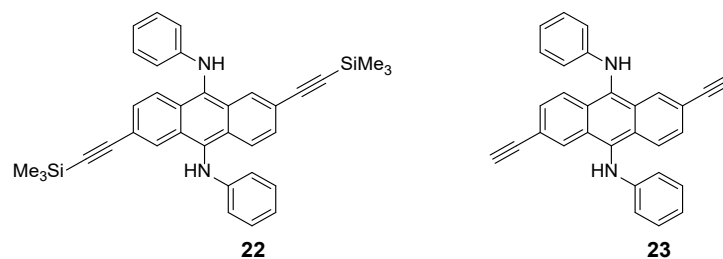

Figure 26. Structures of **22** and **23** anthracene derivatives.

Both compounds **22** and **23** show similar absorption and emission spectra, with compound **23** showing a blue shift in the emission (red) with respect to compound **22** (Figure 27B), which is attributed to the lack of the TMS donating group. The strong absorbance band in **22** (Figure 27A) at 250–340 nm is mainly attributed to n-π* (N-Ph) and π-π* transitions, whereas the weak absorbance at 410–550 nm is attributed to the π-conjugation over the entire molecule and across the nitrogen (N) atom. In addition, both compounds were not sensitive to the solvent polarity, but it was strongly temperature dependent (Figure 27C). As the temperature was lowered, the fluorescence emission was increased. This is a general trend since, at lower temperature, the molecular vibrations are reduced in proportion with nonradiative processes that otherwise diminish the radiative emission due to the competing nonradiative pathways.
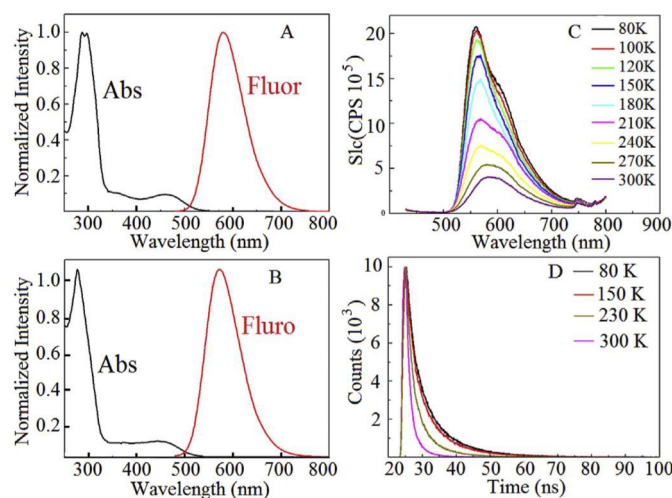

Figure 27. Absorption spectra (black), emission spectra (red) of **22** (**A**), and **23** (**B**) in THF at 25 °C; emission spectra of **22** in solid state at different temperature (**C**) and fluorescence lifetime of compound **22** at variable temperature in solid state (**D**) Reprinted with permission from Ref. [78]. Copyright 2019, Elsevier B.V.

So far, by decorating the anthracene moieties with different functional groups, their photochemical properties change accordingly. This is mainly because their electronic properties and inter-/intramolecular interactions change as well. Nevertheless, this way of modifying the anthracene building blocks sometimes is not straightforward due to difficulties encountered during the synthesis and the time required and the expenses.

Another way of changing their photophysical properties, specifically in the solid state, is by controlling the chromophore packing. Just as in the case of chemical modification, this method can also lead to the desired luminescent properties because in the solid state, the photophysical properties depend on the total collective rather than the single

molecule [79,80]. To study the influence of chromophore arrangement on the photophysical properties in a systematic way, Zhang et al. [81] synthesized four different anthracene derivatives with two of them having a flexible (**24** and **25**) and the other two (**26** and **27**) a rigid structure due to conjugation (Figure 28).
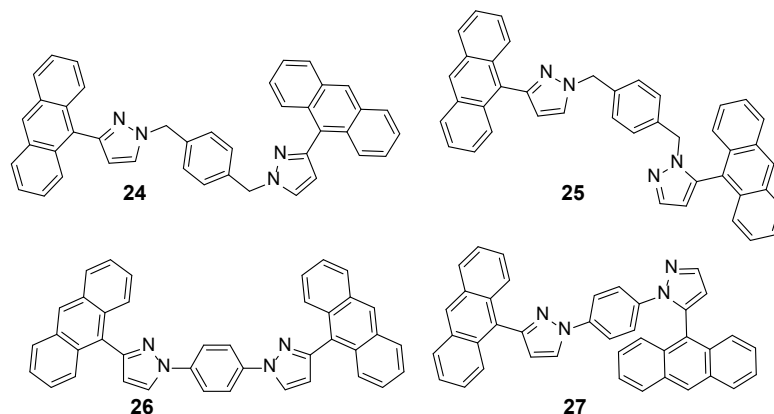

Figure 28. Anthracene derivatives **24**–**27** structures. Adapted with permission from Ref. [81]. Copyright 2009, American Chemical Society.

In solution, all four compounds showed similar well-structured absorptions in the region of 325–420 nm, attributed to the π-π* transition of the anthracene moiety. They differed, however, slightly in the extinction coefficient, with compound **26** having a stronger absorption (Figure 29a). Besides, compounds **24**–**27** showed similar fluorescent emission under the same conditions (diluted chloroform), displaying only a weak effect induced by the anthracene position relative to the pyrazole moiety (Figure 29b).
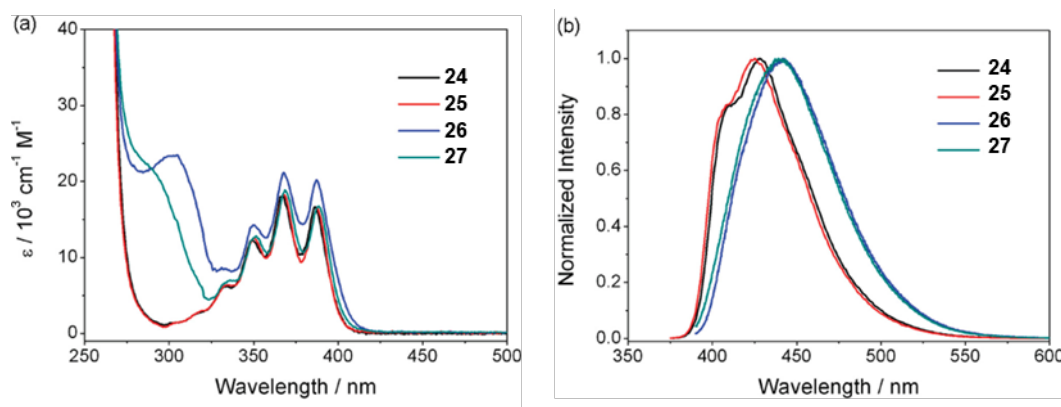

Figure 29. UV−VIS absorption (**a**) and fluorescence spectra (**b**) of compounds **24**–**27** in CHCl$_3$ (3 × 10^{-6} M). Adapted with permission from Ref. [81]. Copyright 2009, American Chemical Society.

However, in contrast to the solution studies, compounds **24**–**27** showed very different emission spectra in the solid state. More interestingly, their emission does not only differ among the different compounds, but it also differs even between the same compounds that can have different crystal packings. This difference in the emission properties is mainly due to different arrangement in the crystal structure as we discussed above due to different crystallizing conditions. For instance, the authors could synthesize two different crystals of compound **24** (**24a** and **24b**). **24a** shows a red shift with the emission lying in the green region (λ_{max} = 515 nm), whereas **24b** crystals emit in the blue region (λ_{max} = 424 nm). The different photophysical properties of the same compound with different structures are almost exclusively attributed to different crystal arrangements. Indeed, compound **1a** shows π-π interactions between the anthracene building blocks, whereas **24b**

does not show such interactions. The other three compounds show a similar behavior to compound **24** except compound **25**, where the fluorescent emission for **25a** and **25b** was almost overlapping, which can be explained by closely similar crystal packing (Figure 30).
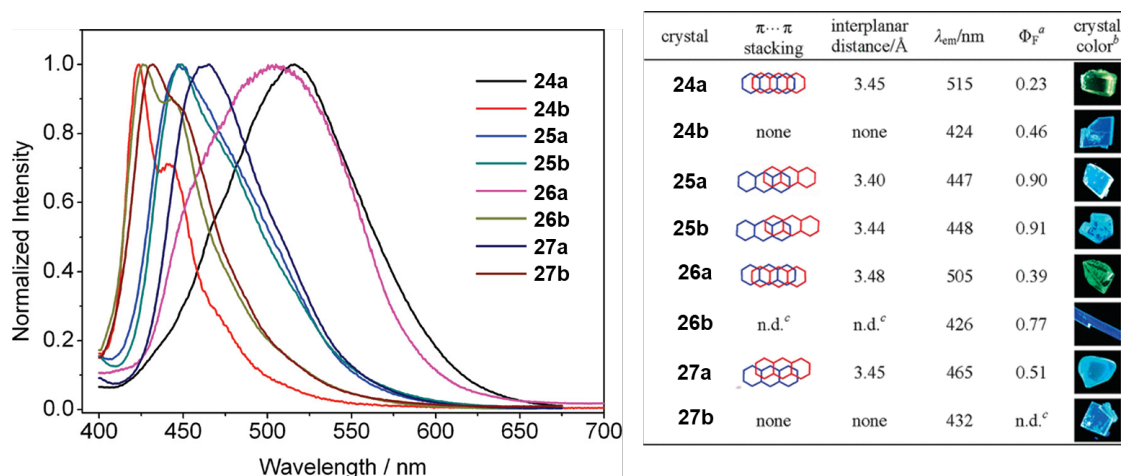

crystal	$\pi\cdots\pi$ stacking	interplanar distance/Å	λ_{em}/nm	$\Phi_F{}^a$	crystal color[b]
24a		3.45	515	0.23	
24b	none	none	424	0.46	
25a		3.40	447	0.90	
25b		3.44	448	0.91	
26a		3.48	505	0.39	
26b	n.d.[c]	n.d.[c]	426	0.77	
27a		3.45	465	0.51	
27b	none	none	432	n.d.[c]	

Figure 30. Solid-state emission (**left**), crystal packing of compounds **24–27** and their photophysical properties (**right**). Adapted with permission from Ref. [81]. Copyright 2009, American Chemical Society.

1.3.3. J-Aggregate

Organic molecules, such as dyes, usually aggregate in highly concentrated [82] solution or in the solid state. This tendency of aggregation affects the photophysical properties of chromophores capable of absorbing and emitting light. The effect in the photophysical properties is mainly caused by π-π stacking and hydrogen bonding interaction, leading to the formation of J- and H-aggregates. Depending on the chromophore structure, and the possibility to form hydrogen bonding, the emission from the solid state sometimes is less intense [83,84] than in solution. However, this is not always the case as it is known that some fluorescence is quite intensive in the solid state. The reason behind that comes from the fact that the structural conformation of the chromophore in the solid state is "frozen", allowing for more conjugation. At the same time, due to the rigidity, there will be less vibration, which otherwise can lead to loss of energy to the environment. These phenomena are attributed to the formation of J- and H-aggregates [85].

J-aggregates are typically characterized by narrow intense bathochromic (red) shifted absorptions, whereas H-aggregates are shifting opposite (H-aggregate, Table 2, Figure 31). Some of their important and distinguishable photophysical properties are given in the table below.

Table 2. J- and H-aggregates' properties.

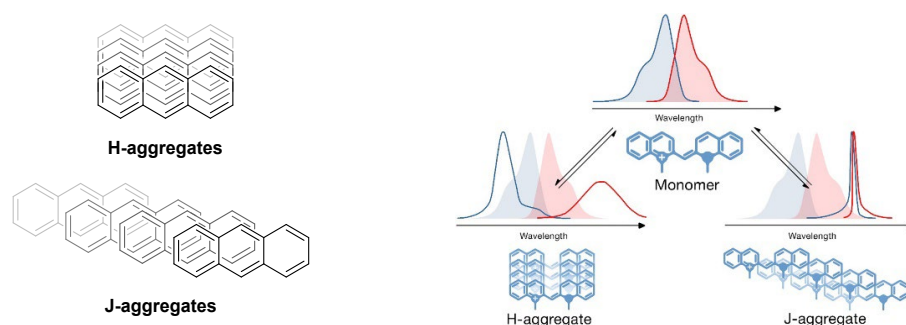| Compd.	Absorbance	Absorbance Intensity	Emission	Emission Intensity	Crystal Packing
J-aggregate	Bathochromic (red) shift	High	Sharpening	High	Side by side
H-aggregate	Hypsochromic (blue) shift	High	Broadening	Low	Face to face

Figure 31. Possible H- and J-aggregate of anthracene (**left**) and schematic representation of the changes in absorption (blue) and fluorescence (red) for cyanine dye monomers (**right**) Reprinted/adapted with permission from Ref. [86]. Copyright 2017, iop Publishing Ltd.

While such effects have been observed by many research groups, we will herein provide some selected cases. For instance, Xiao et al. [87] used two simple anthracene derivatives, DBA (9,10-dibromoanthracene) **4** and DCNA (9,10-dicyanoanthracene) **28**, to synthesize anthracene-derived nanowires (Figure 32) for applications in nanoscience and nanotechnology [88–90].
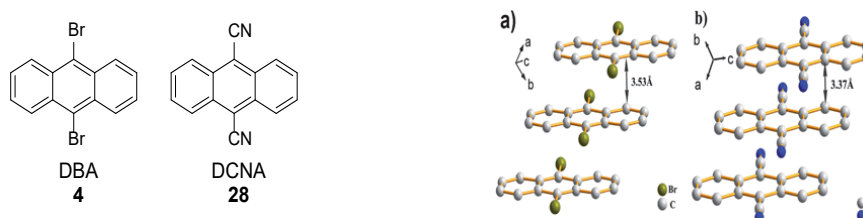

Figure 32. The single-crystal structures of (4) DBA (**a**) and (28) DCNA (**b**). Adapted with permission from Ref. [87]. Copyright 2017, IOP Science.

The prepared nanowires of DBA and DCNA in aqueous solution showed a bathochromic shift both in the absorption and in the emission spectrum, which implies the formation of J-type aggregates, hence slight offset parallel arrangements between the aromatic systems (Figure 33). However, the emission intensities were drastically decreased in the case of the DBA compound due to the heavy atom effect (Figure 33a), whereas the emission of DCNA was stronger than that of DBA (Figure 33b).
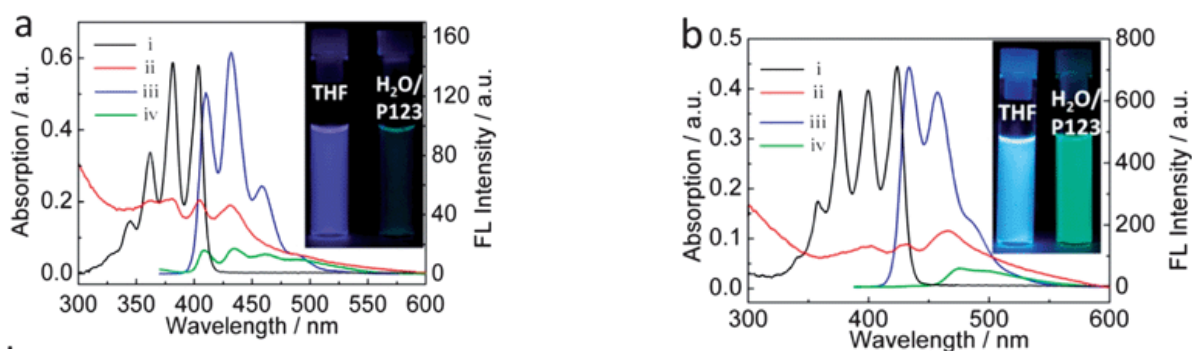

Figure 33. (**a**): UV–VIS spectra of DBA in (i) THF and (ii) aqueous solution. Emission spectra of DBA in (iii) THF and (iv) aqueous solution. (**b**) UV–VIS spectra of DCNA in (i) THF and (ii) aqueous solution. Emission spectra of DCNA in (iii) THF and (iv) aqueous solution. Adapted with permission from Ref. [87]. Copyright 2017, IOP Science.

9-Phenylanthracenyl is modified with rhodamine derivatives, such as tetramethyl rhodamine (TMR) or the silicon-based rhodamine (Si-TMR), to obtain **29**, **30**. Ref. [91]

leads to the formation J-aggregates in aqueous halide ion solution, even though the rho-damine derivatives are known to usually form H-type aggregates under similar conditions [92] (Figures 34 and 35).
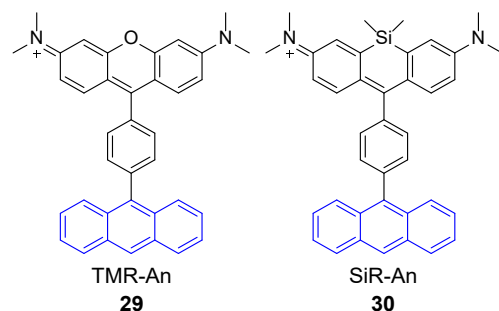

Figure 34. Chemical structures of TMR-anthracene (**left**) and Si-TMR-anthracene (**right**).
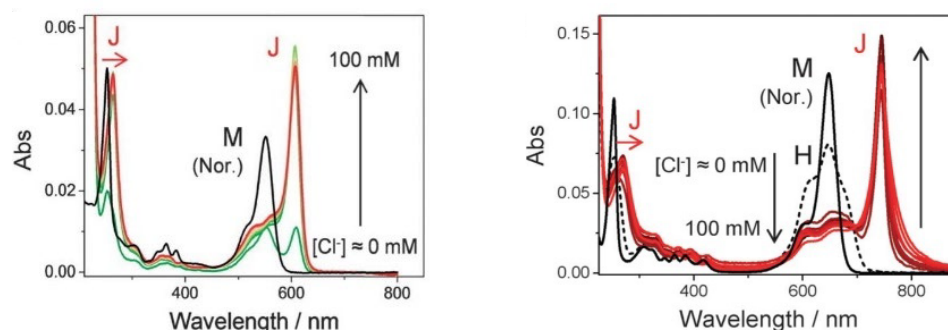

Figure 35. (**Left**) TMR-An monomer (**29**) in methanol (black) and changes in the absorption spectra upon the addition of NaCl from 0 to 100 mM to the TMR-An (**29**) in Milli-Q water (green to red). (**Right**) Normalized absorption spectra of SiR-An (**30**) monomer in methanol (black) and changes in absorption spectra (dashed black line to red). M and J indicate the absorption from the monomer and J-aggregates. Reprinted with permission from Ref. [91]. Copyright 2015, The Royal Society of Chemistry.

Aggregates with photophysical properties typical for that of the J-type aggregates are also reported by An et al. [85]. Addition of water to a THF solution of **31** led to the formation of nanoparticle-sized aggregates, which showed a red shift in both absorbance (Figure 36a) and emission (Figure 36b) with an enhancement of the intensity of the latter. Figure 36 depicts the chemical structure of CN-MBE (left) and J-aggregate formation inducing enhanced emission (right) [85].

The formation of the J-type aggregates is attributed mainly to the presence of the CN group, which apparently does not allow face-to-face aggregation due to steric effects [93], thus leading to the formation of head-to-tail J-aggregates.
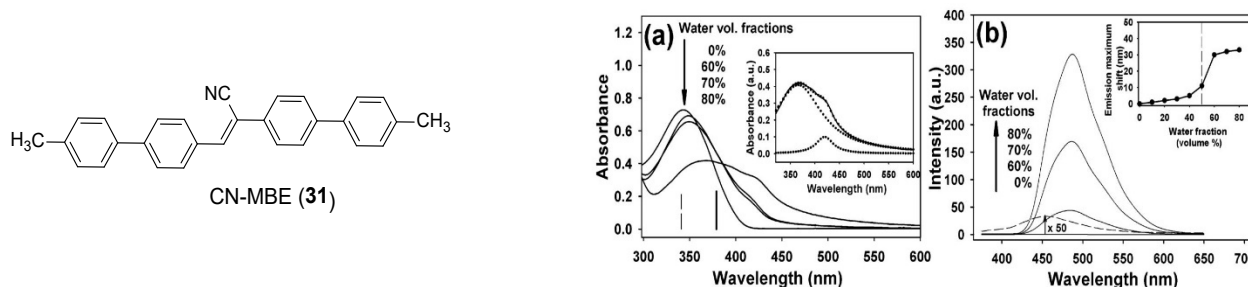

Figure 36. Chemical structure of CN-MBE (**left**) and J-aggregate formation inducing enhanced absorbance (**a**) emission (**b**) Reprinted with permission from Ref. [85]. Copyright 2002, American Chemsitry Society.

In 2009, Swager et al. [94] synthesized different fluorescent macrocycles based on 1,3-butadiyne-bridged dibenz [a,j]anthracene, and by studying their photophysical properties, they observed the formation of J-aggregates in highly concentrated solution and in thin films (Figure 37).
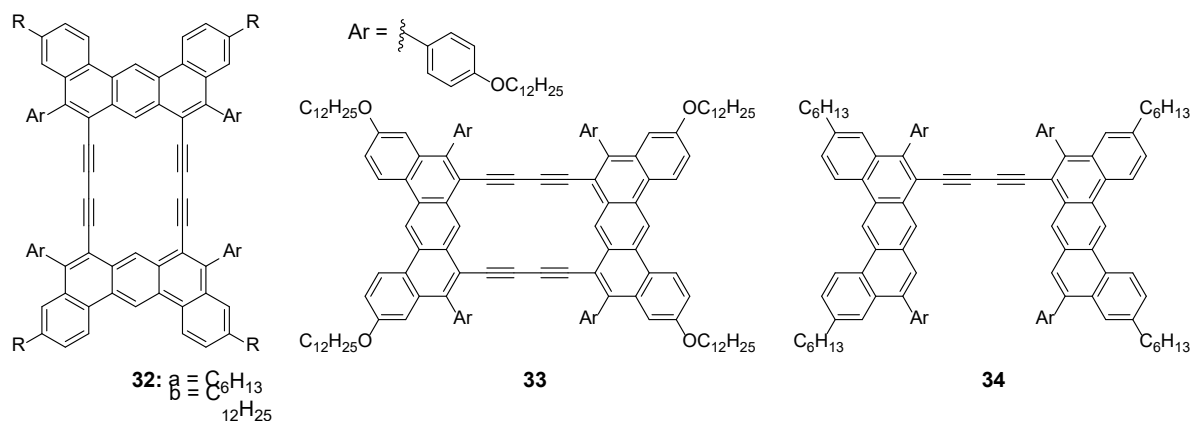

Figure 37. Chemical structure of anthracene derivatives. Reprinted with permission from Ref. [94]. Copyright 2009, American Chemistry Society.

The resulting anthracene-based macrocycles were used to study their photophysical properties using UV–VIS and fluorescence spectroscopy. All four compounds (**32a**, **32b**, **33**, and **34**) showed similar absorption spectra, with compound **34** differing slightly more, due to the larger difference in its chemical structure compared with its analogues, as **34** was lacking the cyclic structure. Compound **33** showed a slight red shift relative to **32a** and **32b** (**32a** and **32b** showed similar absorption spectra), which comes most probably from the presence of the alkoxy groups, whereas compound **34**, due to the lack of the cycle and reduced conjugation, led to a slightly blue-shifted absorption. In addition, compound **34** showed a larger Stokes shift, and this is attributed to the lack of rigidity and higher flexibility as noncyclic compound (Figure 38, left). A bathochromic shift, high-intensity and narrow emission peaks, and small Stokes shifts found for a film of compound **32a** (red) compared with that of **32a** in solution (blue) clearly indicate the formation of J-aggregates [94] (Figure 38, right).
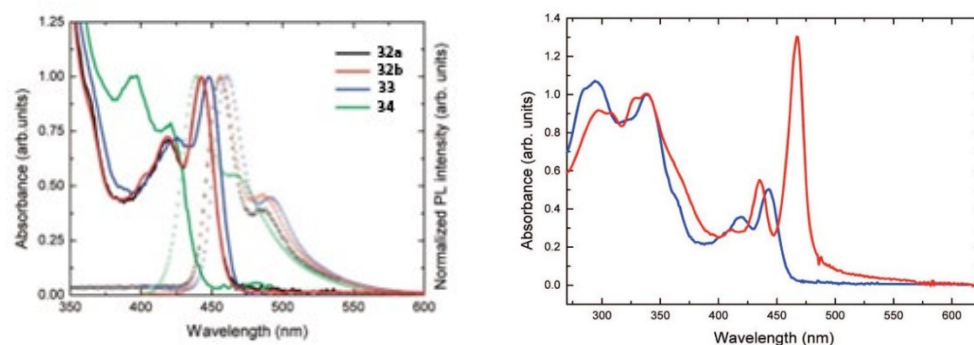
Figure 38. Normalized absorbance (solid lines) and emission (dotted lines) spectra of **32a**, **32b**, **33**, and **34** in chloroform (left) and absorption spectra of **32a**, solution (blue) vs. film (red) (right). Ref. [94]. Copyright 2009, American Chemistry Society.

Another interesting work concerning the J-type aggregates and their photophysical properties was published by the group of Sakar in 2018. In order to understand the photochemical properties of twisted fluorescent organic compounds, they synthesized two twisted biaryl compounds **36** BA and DCBA **37** and compared them with monoaryl AN and CA [95] (left).

The formation of J-type aggregates was confirmed by a red shift in absorbance (Figure 39a,b), but interestingly, they showed a blue shift in the emission spectrum (Figure 40a,b). This could be explained by the presence of a C–C bond in **37** between the anthracene units, which can induce a change in the geometry during the self-assembly process, which then suppresses the charge transfer state, thus causing a blue shift and lowering the emission efficiency (Figure 40).
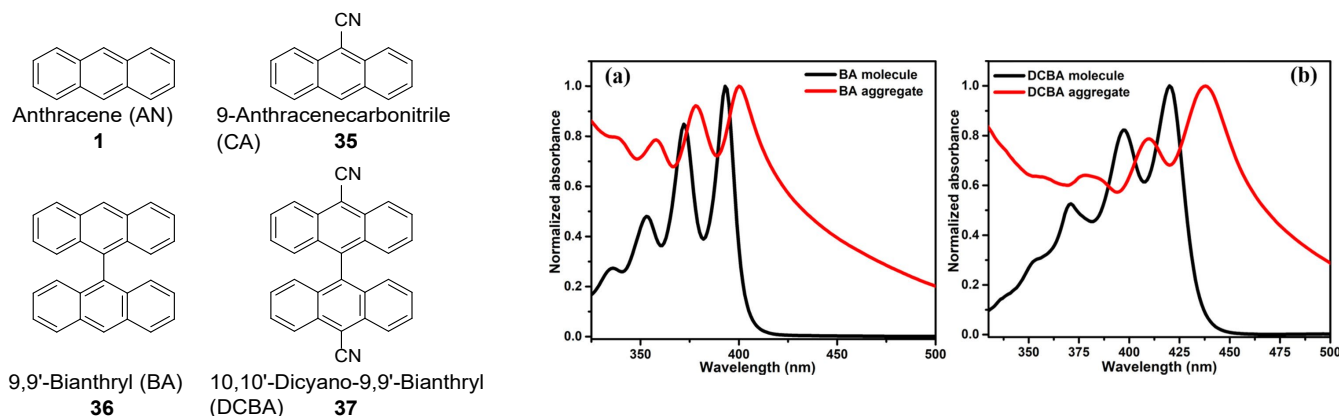

Figure 39. Structure of derivate anthracene (**left**) and normalized absorption spectra of (**a**) BA (**36**) in molecular form in DMSO and aggregated form in water–DMSO mixture and (**b**) DCBA (**37**) in molecular form in DMSO and aggregated form (water–DMSO mixture) (**right**). Reprinted with permission from Ref. [95]. Copyright 2018, American Chemical Society.
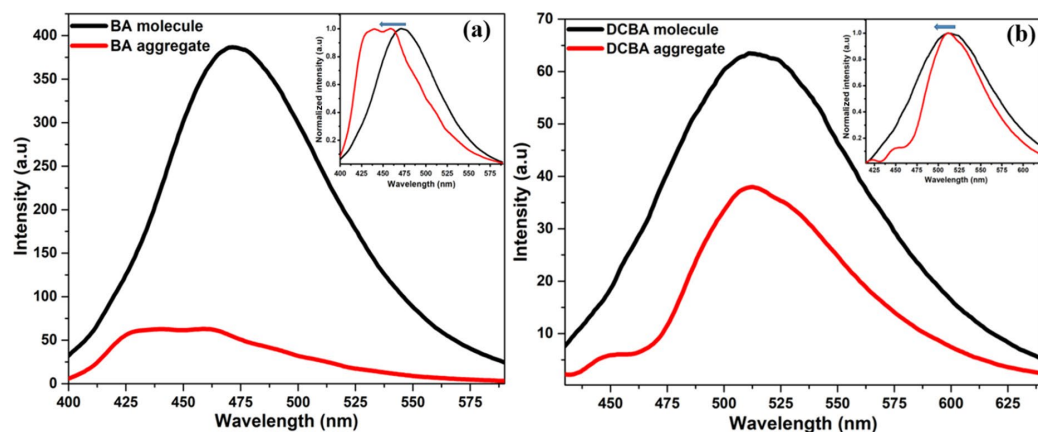
Figure 40. Emission spectra of (**a**) BA (**36**) and (**b**) DCBA (**37**) in molecular form in DMSO (black) and aggregated form in water–DMSO mixture (red). The inset provides the normalized emission spectra of BA and DCBA in the molecular and aggregated states. Reprinted with permission from Ref. [95]. Copyright 2018, American Chemical Society.

1.3.4. H-Aggregate

Additionally, H-aggregates can be formed in concentrated solution and in the solid state. Nevertheless, their perfect head-to-head (face to face) interaction makes them different from other aggregation types (e.g., J-type), thus leading to blue (hypsochromic) shifts in the absorbance spectrum [96]. A typical example of H-type aggregates is shown by Gierschner et al. [97,98] using different derivatives of distyrylbenzene **38** (DSB), **39** F$_{12}$DSB, and **40** *t*-Bu$_4$DSB (Figure 41).
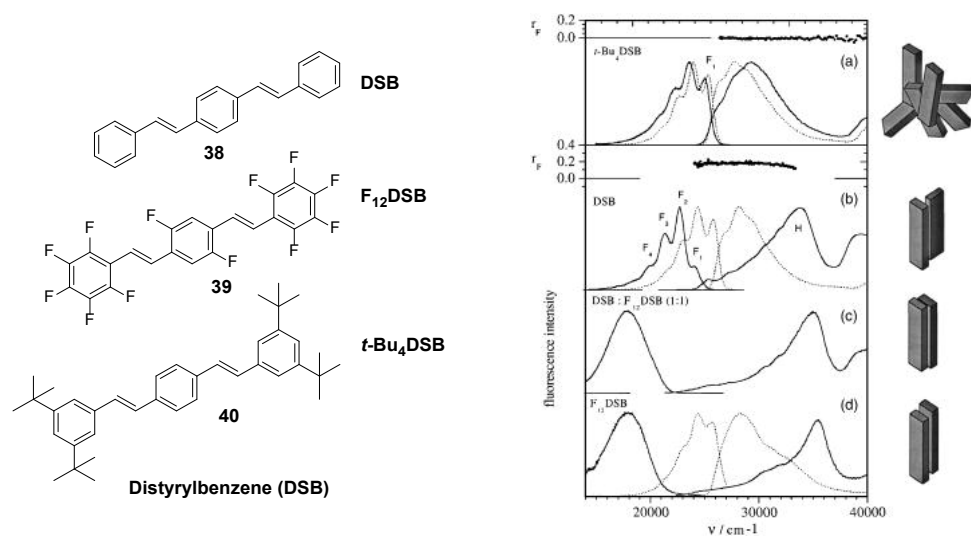
Figure 41. Emission (**left**)/absorbance (**right**) of distrylbenzene (DSB) nanoparticles: (**a**) *t*-Bu$_4$DSB, (**b**) DSB, (**c**) cocrystalized DSB: F$_{12}$DSB, and (**d**) F$_{12}$DSB. Dashed lines are spectra in solution (n-hexane) for comparison. Reprinted with permission from Ref. [97]. Copyright 2005, AIP Publishing.

The investigation showed that distyrylbenzene **38** (DSB) arranges in a herringbone manner, with the long axes oriented in parallel, but the short axes nearly perpendicular to each other. In contrast, polyfluorinated distyrylbenzene **39** and the 1/1 mixture of DSB: F$_{12}$DSB cocrystals arrange face-to-face via π-π stacking in the solid state, thus as H-aggregates. Photophysical investigation showed that compounds arranged face-to-face DSB: F$_{12}$DSB and F$_{12}$DSB show strong interactions and express a strong blue shift in the absorption spectrum as well as an unstructured strong red-shifted excimer-like spectrum, compared with DSB alone, which shows a similar well-structured emission spectrum to the one in solution due to weak intermolecular vibronic coupling (Figure 41).

In general, the H-type aggregates are known to be less efficient in photoluminescent emission due to their high/strong interaction between the aggregates in the solid state. However, Wang et al. [99] could efficiently increase the emission intensity of tetracene **41** and pentacene **42** (guest compounds) by doping into trans-DSB compound **38** (host compound). The crystal structures of tetracene and pentacene induce self-quenching, leading to a very low emission efficiency due to the H-aggregates and strong vibronic interactions, whereas doping these two compounds into DSB increases the emission efficiency by up to 74% due to the lack of intermolecular aggregation. Furthermore, controlling the amount of doped tetracene and pentacene leads to the emission of different colors. Undoped DSB crystals give blue emission, whereas the doped crystals with tetracene and pentacene give green and red emissions, respectively (Figure 42).

Figure 42. Structures of DSB (**38**), tetracene (**41**), and pentacene (**42**). Absorption (**a**) and emission (**b**) spectra of trans-DSB crystal, tetracene-doped trans-DSB crystal, and pentacene-doped trans-DSB crystal. Reprinted with permission from Ref. [99]. Copyright 2009, American Chenistry Society.
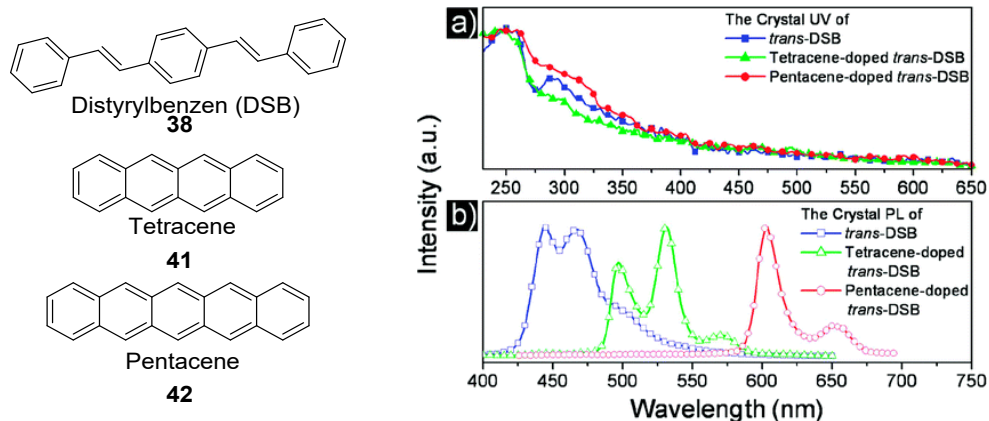
Similar to the work of Gierschner et al., where he used substituted distyrylbenzene (DSB) **38** to study the effect of the substituents (fluorine, *t*-Bu) on the photophysical properties in both solution and solid state, Sun et al. [100] used fluorine-substituted distyrylanthracene (DSA) **43** for the same purpose (Figure 43).

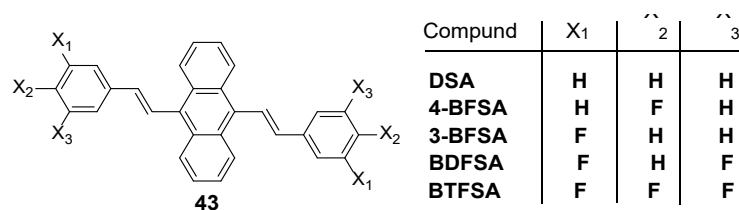| Compund	X_1	X_2	X_3
DSA	H	H	H
4-BFSA	H	F	H
3-BFSA	F	H	H
BDFSA	F	H	F
BTFSA	F	F	F

Figure 43. Chemical structures of DSA derivatives.

His findings were in line with the work of Gierschner and others, since during the investigation, he found different photophysical properties depending on the degree and position of fluorination. Hence, DSA, 4-BFSA, 3-BFSA, BDFSA, and BTFSA express different photophysical properties due to different packings. In addition, DSA derivatives exhibited solvatochromic effect; red-shift emission is observed by increasing the solvent polarity [100] (Table 3).

Table 3. Photophysical properties of DSA derivatives.

Compd.	Solution		Solid		PL (nm) in THF/H_2O (%)					PL (nm) in Different Solvents [a]				
	Abs	F_{PL} [b]	PL	F_{PL} (%)	0	30	50	70	90	HEX	TOL	DCM	ACT	Me
DSA	410	52	508	14	556	571	568	491	506	545	559	578	586	587
4-BFSA	410	53	502	18	557	561	576	482	480	545	558	567	585	586
3-BFSA	410	57	518	49	558	566	567	491	504	545	555	576	582	584
BDFSA	412	59	448	62	555	566	567	491	505	542	553	560	568	571
BTFSA	413	56	579	39	509	508	508	508	544	502	506	510	505	501

[a] HEX: n-hexane; Tol: toluene; Me: methanol; DCM: dichloromethane; ACT: acetone. [b] Solution fluorescence quantum yield estimated by using 9,10-diphenylanthracene as the standard.

1.4. Excimers

Aggregates of two atoms/molecules that can be formed only in the excited states are called excimer (excited dimer). Furthermore, this species can only exist in the excited state because the ground state of the dimer [101] is not energetically favorable [102]. Typically, excimers $[M_A M_A]^*$ are formed when monomer M_A is excited from the ground state to the

excited state M_A^* by absorbing a photon. Then the excited monomer M_A^* forms the excimer $[M_AM_A]^*$ with another monomer M_A from the ground state (Figure 44).

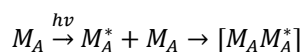$$M_A \xrightarrow{h\nu} M_A^* + M_A \rightarrow [M_AM_A^*]$$

Figure 44. Excimer formation.

This process consists of light absorption, association, emission [103], and dissociation to the ground state (Figure 45a) The photophysical properties of the excimer differ from those of the monomer alone [104], showing a red shift and longer lifetime as well as a structureless emission spectrum (Figure 45b).
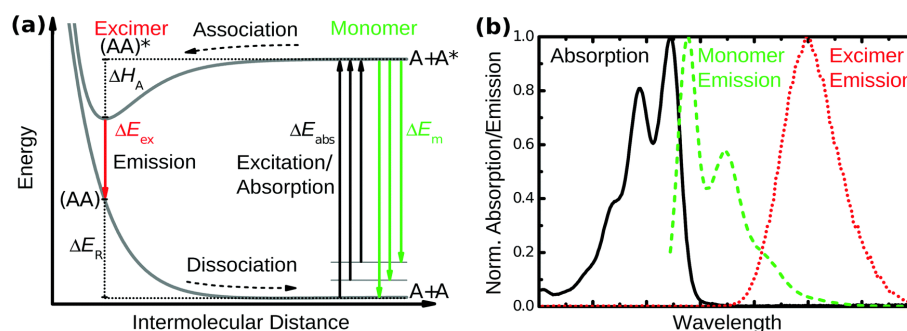

Figure 45. (**a**) Energy levels and possible process for the formation of the excimers, * Exciting state; (**b**) normalized spectra of absorption (black), monomer emission (green), and excimer emission (red). Reprinted with permission from Ref. [103]. Copyright 2015, Royal Society of Chemistry.

Anthracene, on the other hand, might have five possible excimers: normal dimers [105], offset, twisted [106], T-shaped, and twisted plus end-overlapped dimers (Figure 46) [107,108].
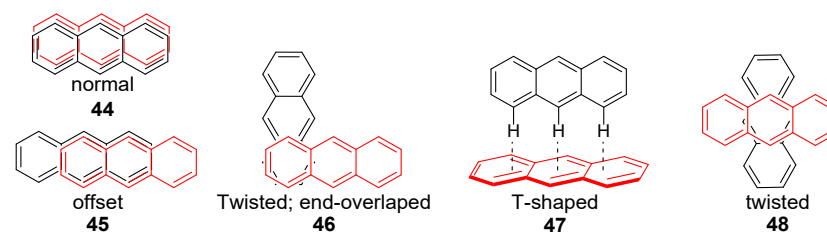

Figure 46. Five possible anthracene excimers.

To better understand the relationship between the structure and the photophysical properties of an excimer, it is of high importance to find a real model, which forms a single and pure excimer. One can think of simple aromatic compounds such as benzene, naphthalene, or anthracene, but the problem with such compounds is that they usually form infinite herringbone arrangements, which are far from what is indeed needed.

Nevertheless, such an excimer with a similar emission in solution and in the solid state is formed by the monosubstituted 2-(anthracen-9-yl)thianthrene (2-TA-AN) **49** presented by the group of Gao et al. [109,110] (Figure 47).
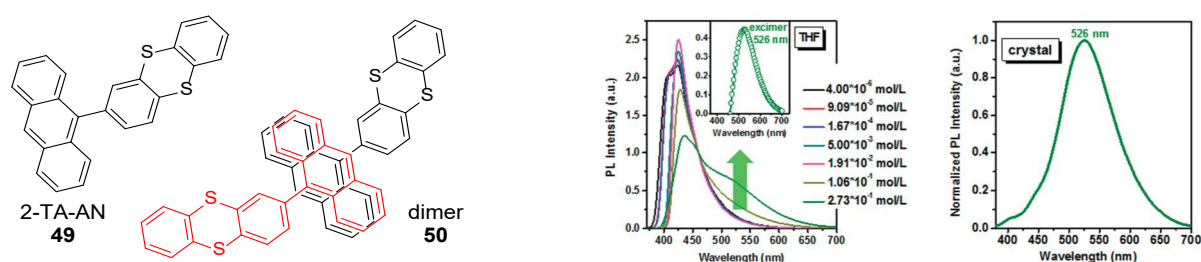
Figure 47. PL spectra recorded for 2-TA-AN in THF solutions with increasing concentration and in crystal form. Molecular structure of 2-TA-AN in solution and the intermolecular packing. Reprinted with permission from Ref. [109]. Copyright 2018, Royal Society of Chemistry.

The resulting dimer **50** is formed via antiparallel face-to-face stacking, and the discrete dimeric structure is established thanks to the thianthrene substituent, which spatially separates anthracene dimers from each other, thus preventing further aggregation. As shown in Figure 47, the resulting dimer emits in the green region (λ_{max} = 526 nm) versus the monomer, which displays blue emission (λ_{max} = 424 nm) in diluted solution.

A similar approach was followed up by Prasad et al. [111] in order to study the possible excimer formation and the photophysical properties in both solution (DCM) and solid-state thin films. For that purpose, they synthesized different anthracene derivatives functionalized with amino alkyl chains (**51** octyl, **52** dodecyl, **53** octadecyl, and **54** *p*-butylaniline) (Figure 48, Table 4).
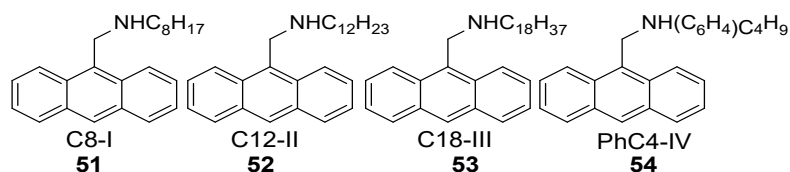

Figure 48. Anthracene-derived structures. Reprinted with permission from Ref. [111]. Copyright 2010, Elsevier.

Spectroscopic investigation showed excimer formation (Figure 49, right). However, in solution, only fractions of the excimers were formed contrary to that of the solid state, where exclusively excimer formation was observed, which can be explained by a close rigid packing of anthracene moieties. In addition, glassy thin films were obtained upon fast cooling to room temperature after heating the solid thin films, thus exhibiting a plastic crystalline phase. A closer look into the packing showed discotic (rectangular columnar) arrangement (Figure 49, left).
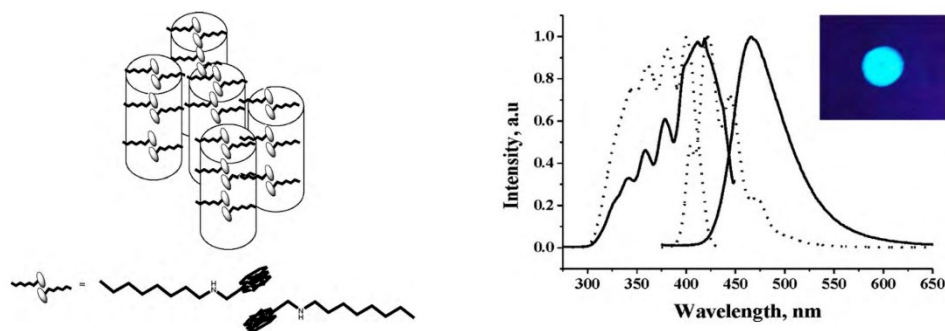
Figure 49. Cartoon representation showing the rectangular columnar arrangement in **51** (**left**). Excitation (**left**) and emission (**right**) spectra of anthracene (dot) and **53** (solid) at solid thin film after heat treatment. Inset shows a UV-illuminated photo of **53** in solid thin film on a glass slide at room temperature, providing anthracene excimer emission (right). Anthracene-derived structures. Reprinted with permission from Ref. [111]. Copyright 2010, Elsevier.

Nevertheless, comparing the photophysical properties of the different anthracene derivatives used revealed slight differences due to the different length of the alkyl chain substituents.

Table 4. The photophysical properties of 51, 52, 53, and 54 in dichloromethane. "Reprinted with permission from Ref. [111]. Copyright 2010, Elsevier".

Compound	l_{max}^{abs}/nm	l_{max}^{PL}/nm (L)	F	Excimeric t, ns (Relative Amplitude, %)
51	262, 357 365, 384	420, 442, 472	0.26	$\tau_1 = 3.52\ (22.34)$ $\tau_2 = 7.46\ (77.66)$
52	264, 355 366, 384	420, 444, 474	0.22	$\tau_1 = 2.78\ (33.79)$ $\tau_2 = 5.56\ (04.76)$ $\tau_3 = 11.10\ (61.44)$
53	264, 355 365, 382	418, 442, 471	0.16	$\tau_1 = 2.72\ (19.12)$ $\tau_2 = 7.28\ (80.88)$
54	263, 356 364, 384	420, 443, 473	0.33	$\tau_1 = 2.31\ (32.89)$ $\tau_2 = 7.07\ (67.11)$

In 2014, Feng et al. [112] reported on anthracene-based excimer emission with sensing properties for pyrophosphates (PPi). The resulting excimer after complexation of PPi with zinc-based anthracene complex led to a red-shifted emission, indicating its presence (Scheme 9).
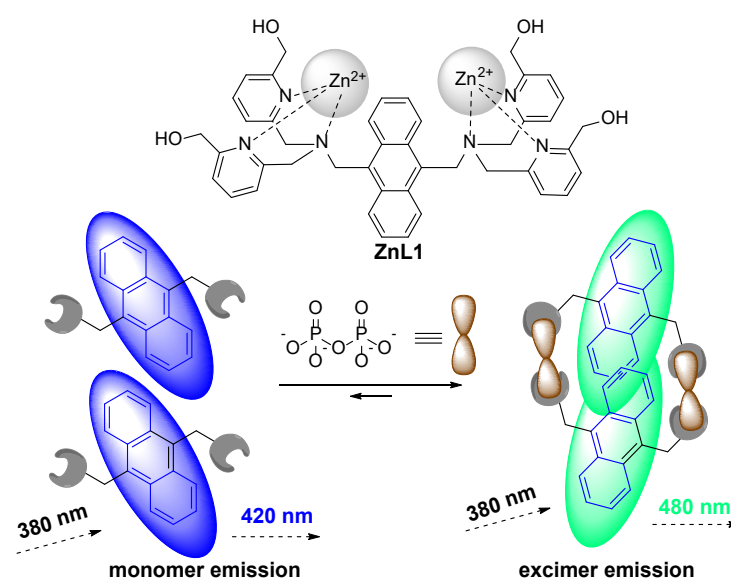
Scheme 9. Complex of ZnL1 and PPi sensing. Reprinted with permission from Ref. [112]. Copyright 2020, American Chemical Society.

The monomer itself, when exposed to 380 nm, emitted in the blue region (420 nm), whereas addition of PPi led to the formation of excimer, which, under the same irradiation wavelength, emitted at 480 nm in the turquoise region (Figure 50).
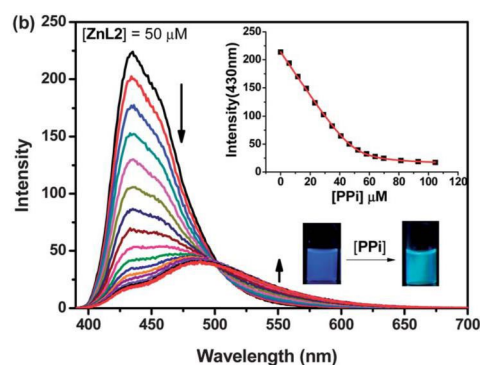
Figure 50. Fluorescent intensity changes (decreases) at 430 nm as a function of [PPi] and increases at 480 nm excimer emission. Reprinted with permission from Ref. [113]. Copyright 2011, RSC Publishing.

1.5. Exciplexes

Exciplexes (excited complex) $(M_A M_B)^*$ are chemical species formed when one monomer (M_A) in the excited state forms a complex with another (different) monomer M_B in the ground state (Figure 51).

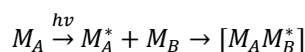$$M_A \xrightarrow{h\nu} M_A^* + M_B \rightarrow [M_A M_B^*]$$

Figure 51. Exciplex formation.

Ideally, exciplex formation requires the use of proper compounds where one of them is an electron donor (HTM—hole transporting material) and the other one an electron acceptor (ETM—electron transporting material) [112].

Exciplexes usually display a red-shifted structureless broad emission spectrum and, therefore, are used as emitters and considered as potential organic light-emitting diodes (OLED) due to their capability of host–guest energy transfer [114,115].

A typical example of an exciplex formation between simple anthracene **1** and dimethyl aniline **55** was observed by Geddes et al. [116] as they found an increase in fluorescence intensity of an unstructured band at 500 nm, while a decrease in intensity of the well-resolved vibrionic structure of the pure anthracene emission was observed (Figure 52). The formation of a charge transfer complex during the irradiation of anthracene diethylaniline mixture was identified to be responsible for exciplex emission.
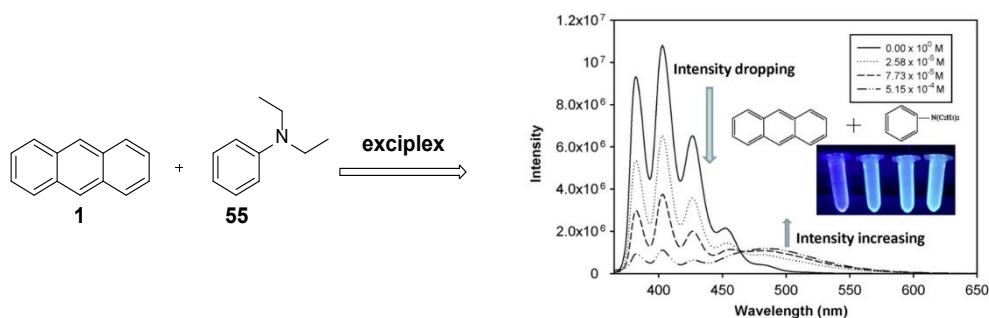
Figure 52. Exciplex formation between anthracene and diethylaniline at various concentrations in toluene. Reprinted with permission from Ref. [116]. Copyright 2011, Elsevier B.V.

Another example of exciplex formation with a broad, structureless, and red-shifted emission compared with the anthracene derivative alone was observed by the group of Chen at al. [117] when exposing a solid thin film of a mixture of anthracene derivative **56** with an amino compound **57** at 50%wt to UV light.

Emission of pure anthracene derivative monomer at λ_{max} = 449 nm was red-shifted to λ_{max} = 482 nm for the mixture with **57** (TAPC = Di-{4-N,N-ditolyl-aminophenyl}cyclohexane) thin films, indicating the formation of the exciplex (Figure 53).

Figure 53. Chemical structure: anthracene derivative (**left**), amino compound (centered), PL spectra of **56** and **56:57** thin films (**right**). Reprinted with permission from Ref. [117]. Copyright 2019, Elsevier B.V.
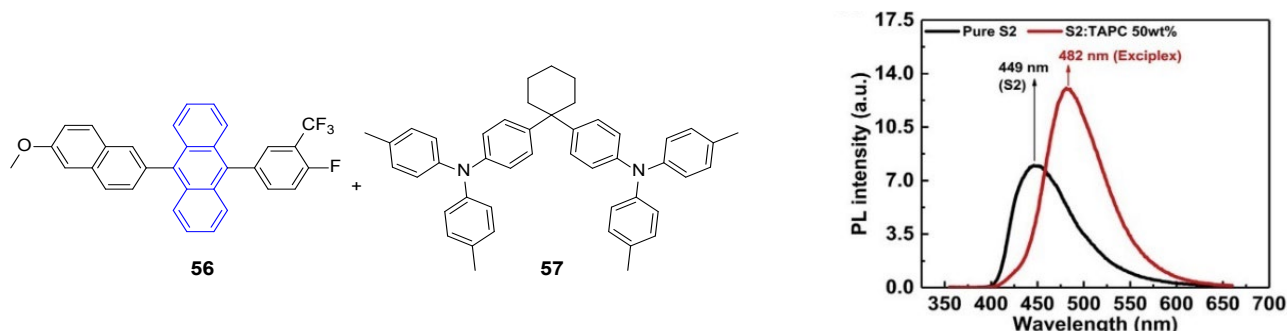
Compounds already known to form exciplexes with anthracene and its derivatives are, e.g., oxygen [118], dienes [119], and amines [120,121]. In 1975, Yang et al. [122] used dimethylaniline (DMA) in order to investigate the photochemistry of anthracene. They found out that in the absence of DMA, the only reaction was the photodimerization of anthracene **9**, whereas in the presence of DMA, competing reactions were occurring, leading to the formation of different products (**58**, **59**, **60**) depending on the concentration of the DMA (Figure 54).
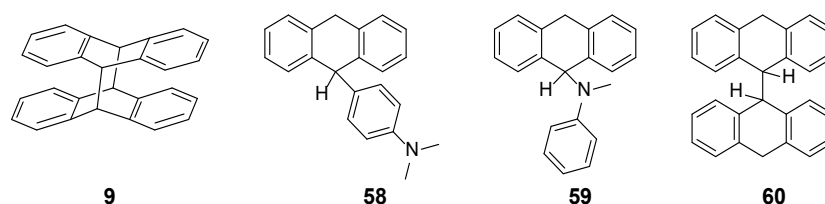
Figure 54. Photochemical products formed in the presence of DMA.

These competing reactions were mainly attributed to electron transfer from the amine to the exited state of anthracene, and the intermediate was the exciplex formed in the excided state between these two compounds [122,123]. In addition to their interesting properties in photoluminescence, exciplexes are known as well to be the "obligatory" [124] intermediate of a photochemical reaction like in the [2 + 2] cycloaddition of 9-cyanophenanthrene **61** with β-methylstyrene **62** (Scheme 10).
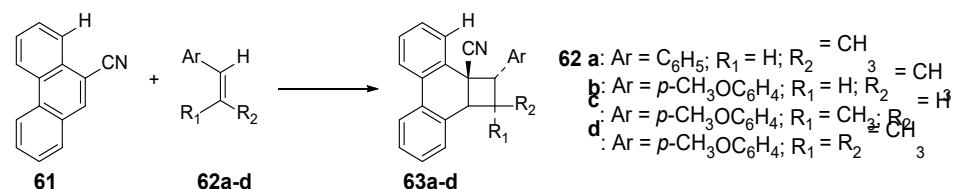
Scheme 10. Example of [2 + 2] cycloaddition through the exciplex intermediate. Adapted with permission from Ref. [124]. Copyright 1974, Chemical Society.

1.6. Dyad Emission

Systems/materials composed of two distinct covalently bound organic/inorganic compounds are known as dyads [125]. Such systems have been intensively investigated

[126] by many research groups for possible applications [127,128]. Ge at al. [129] synthesized the anthracene-appended ferrocene dyad **64** containing the aniline and thiourea donor moieties for sensing Cu(II) and Hg(II) ions (Figure 55). Dyad **64** exhibited a very weak emission at λ_{max} = 395, 416, and 440 nm, respectively. The weakness of emission is attributed to photoinduced electron transfer (PET) from aniline and ferrocene as electron-rich species, quenching the fluorescence of the linked anthracene. However, the addition of metal ions such as Cu (II) and Hg (II) led to the increase in the emission, indicating that the nitrogen atom of aniline and the sulfur atom in thiourea are the binding sites for the metal ion coordination in **65** (Figure 55).
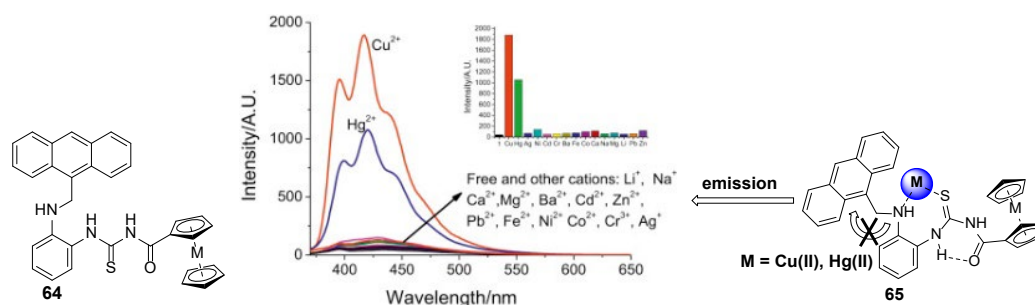

Figure 55. Structure (**left**), emission (**centered**), and binding mode (**right**) of dyad **64.** Reprinted with permission from Ref. [129]. Copyright 2015, Elsevier B.V.

Further, an anthracene-based dyad was published by Tykwinski et al. [130], this time combined with a pentacene unit **66**. The anthracene core was modified at position 9 with different substituents, e.g., H, F, Cl, Br, and CH₃ (Figure 56).
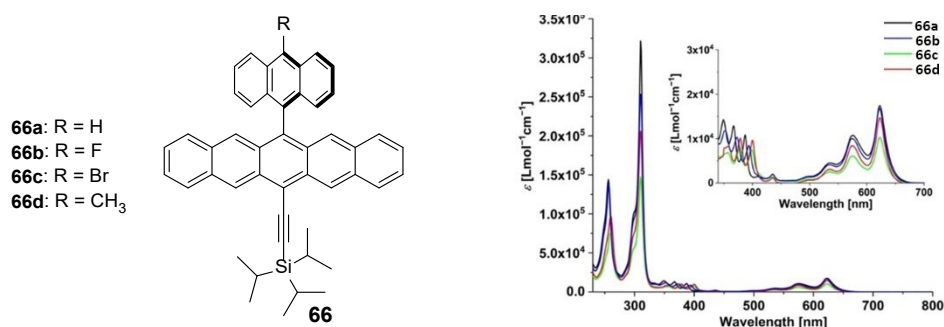
Figure 56. Structure (**left**), UV–VIS absorption spectra of **66a–d** (measured in CH₂ region of 225–800 nm and expansion from 340–700 nm (**right**). Reprinted with permission from Ref. [130]. Copyright 2020, Wiley-VCH Verlag GmbH & Co.

The resulting dyad derivatives showed very similar photophysical properties (Figure 56, right), which could be best explained by the X-ray structures [131] (Figure 57), which were similar regardless of the presence of different substituents on the anthracene. A characteristic absorption band for the pentacene unit was observed at λ_{max} = 310 nm and in the low-energy region at λ = 536, 537, 623 nm, whereas the main absorption band for the anthracene core was observed at λ_{max} = 256 nm, including a series of week absorptions at λ = 349, 367, and 387 nm.
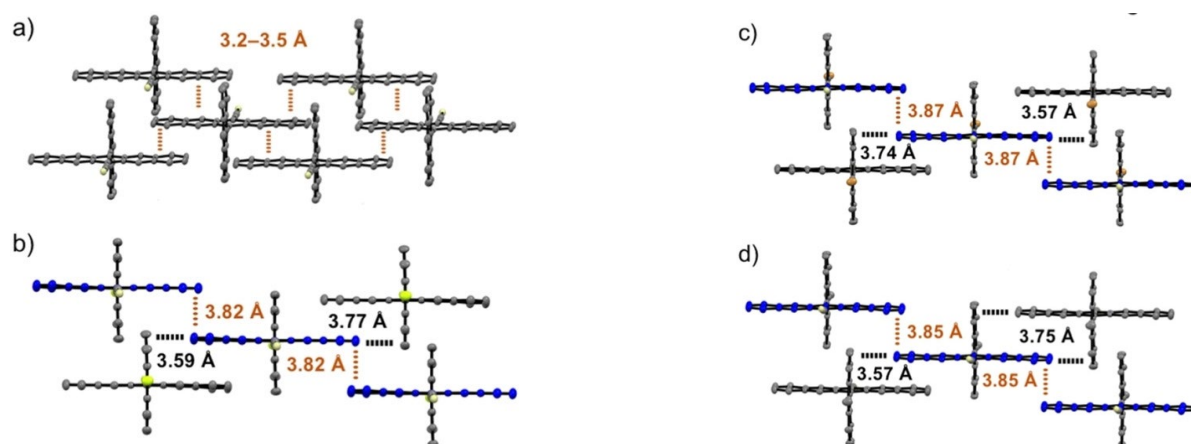
Figure 57. (**a**–**d**) X-ray structures of **66a**–**d**. Reprinted with permission from Ref. [130]. Copyright 2020, Wiley-VCH Verlag GmbH & Co.

In 2019, the group of Chaari et al. [132] synthesized such dyads for very efficient blue light emission, using a nucleophilic substitution reaction between an anthracene moiety and an m-carborane cluster (Scheme 11).
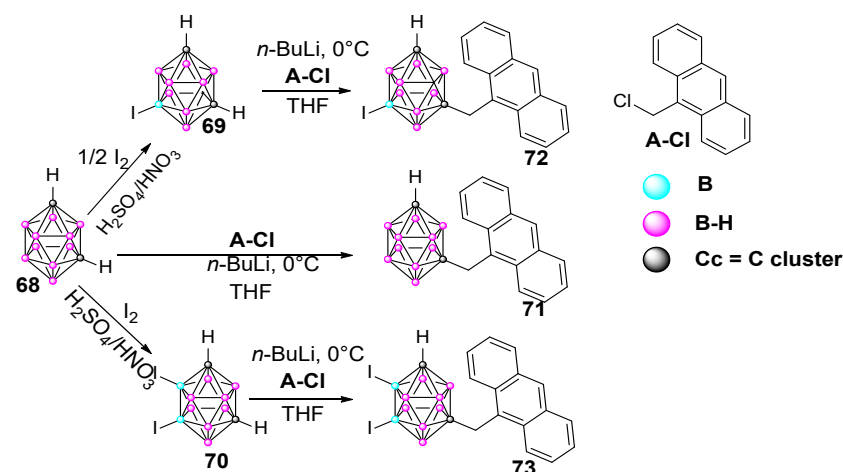
Scheme 11. Synthesis and characterization of anthracenyl-monosubstituted m-carborane derivatives **71**, **72**, and **73**. Reprinted with permission from Ref. [132]. Copyright 2019, The Royal Society of Chemistry.

Dyads **71**, **72**, and **73** show similar well-structured absorption spectra largely attributed to π-π* transitions of the anthracene compound. In addition, these dyads display excellent emission properties showing almost quantitative (95–100%) fluorescence quantum yields in solution for all of them, which is significantly higher than the one containing two anthracene moieties [133]. The high efficiency emission is attributed to the presence of the CH$_2$ linker, which allows a free rotation of the anthracene core (Figure 58a).
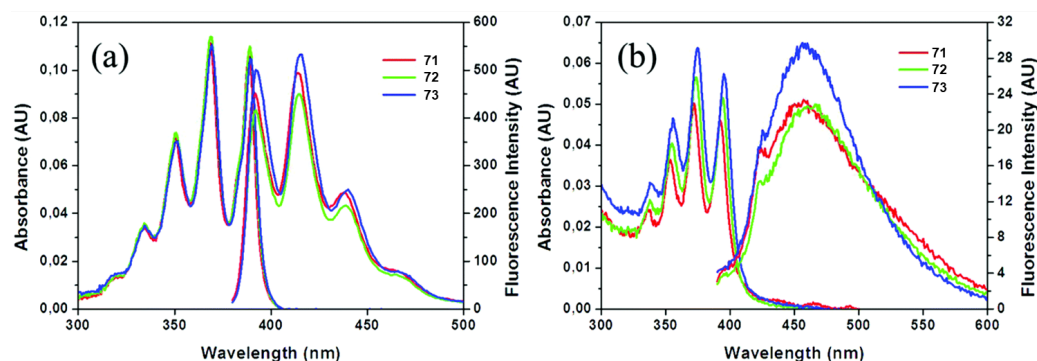
Figure 58. Absorption and emission spectra of **71** (red), **72** (green), and **73** (blue) in THF solutions (**a**) and aggregates (THF/H₂O, 1/99, *v/v*) (**b**). AU: arbitrary units. Adapted with permission from Ref. [132]. Copyright 2019, The Royal Society of Chemistry.

Furthermore, these dyads retained their emission properties in the aggregated state as well (Figure 58b), again thanks to the presence of CH_2 in **71** and iodine in **72** and **73,** which prevents π-π stacking due to steric hindrance (Figure 59).
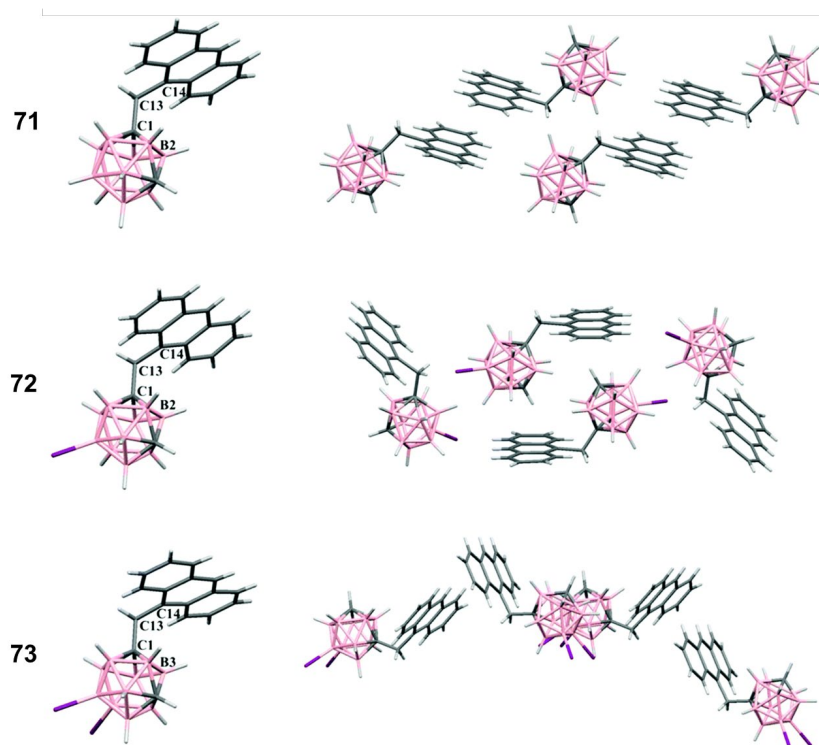
Figure 59. Crystal packing of compounds 71, 72, and 73. Adapted with permission from Ref. [132]. Copyright 2019, The Royal Society of Chemistry.

Crystal structures of compounds **71**, **72**, and **73** were formed to be mainly controlled by the intermolecular interaction between C–H and B–H of carbaborane with anthracene moiety. In addition, compound **71** showed further interaction between hydrogen atoms of –CH_2– groups and anthracene, whereas compound **72** featured further C–H-π interactions (Figure 59).

Thus, intermolecular π-π interactions between the anthracene building blocks were prevented mostly by the interaction of hydrogen atom from the carbaborane cluster and anthracene (Cc–H-A) among weak B–H-I-B interaction. Due to these interesting photophysical properties, these compounds have potential for bioimaging applications.

1.7. Triade Emission

Systems/materials composed of three distinct organic/inorganic (usually π-conjugated organic) compounds are known as triads. Such systems can be used to develop heavy atom-free-triplet photosensitizers [134]. A typical example is given in the work conducted by Xing et al., who synthesized two (**74**, **75**) slightly different triads composed of carbazole (CZ), anthracene (AN), and bodipy (BDP) (Figure 60).

Figure 60. Triad chemical structures (**left**), and TTA upconversion with **75** as the photosensitizer and perylene (Pery) as the acceptor (**right**). Excited with a 510 nm cw laser (50 mW cm^{-2}). c [perylene] = 2.0 × 10^{-5} M, in deaerated dichloromethane, 20 °C. Inset: photographs of **75** alone and the upconversion. Reprinted with permission from Ref. [134]. Copyright 2018, American Chemical Society.
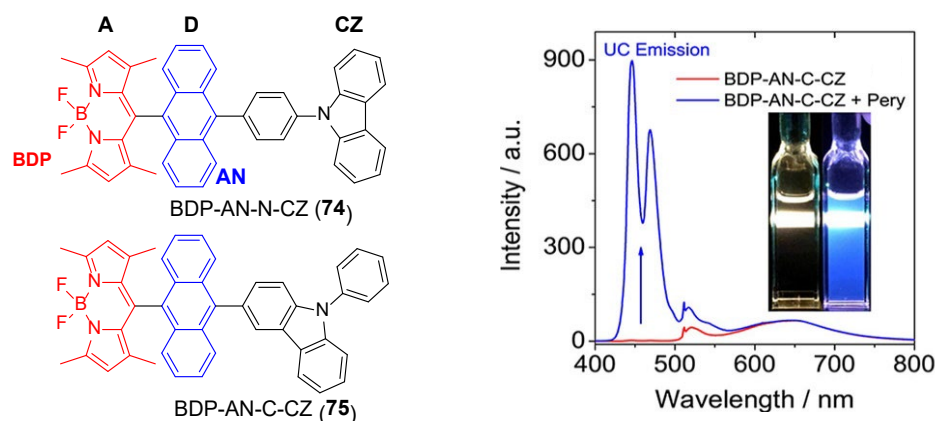
These triads were composed of two donors (CZ and AN) and one acceptor (BDP) organic moieties and linked together in such a way that a sequential electron transfer was possible. Furthermore, in order to study the photophysical properties especially on spin–orbit charge transfer intersystem crossing (SOC-ISC), the position and distance of the carbazole moiety was varied because it is known that substrate modification, e.g., substitution, influences their performances. [135] Such triads were used as triplet photosensitizers for triplet–triplet annihilation (TTA) upconversion (Figure 60, right). The mechanism for triplet–triplet annihilation (TTA) involves an energy transfer between two molecules already in the triplet excited state. This process would allow one molecule to go back to the ground state and the other one to be promoted to higher energy levels [136].

The reactions of proton-coupled electron transfer (PCET) were studied by Hammer-Schiffer et al. [135] using a triad [137] molecule **76** composed of anthracene, phenol, and pyridine building blocks. Using different substituents, they studied first their effect on the decay of a locally excited state (LES) to the ground state (GS) and, second, explained the long-lived charge separation state (CSS) (Figure 61). LEPT stands for local electron–proton transfer.
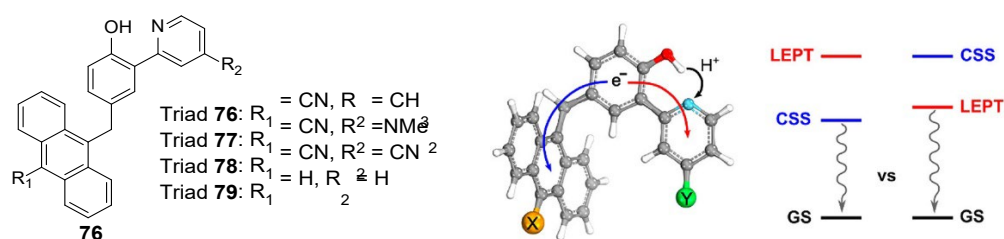

Figure 61. Triads and their chemical structure (**left**), concerted electron transfer from phenol to anthracene and proton transfer from phenol to pyridine (**right**). Adapted with permission from Ref. [137]. Copyright 2019, The American Association for the Advancement of Science.

1.8. Coordination Polymers (CPs)

Coordination polymers (CPs) are supramolecular assemblies [138] formed typically between an organic compound (ligand, electron donor) and an inorganic salt [139] (metal ion, electron acceptor) through noncovalent bonding [140]. CPs and their properties among other factors (e.g., solvents, temperature) are dependent on the nature of the donor and acceptor species, which can lead to the formation of 1D [23,141], 2D [23], and 3D [142] structures showing different chemical, physical, and photophysical properties. Since their introduction, such CPs, especially those based on fluorescent building blocks, have found many applications, thanks to their capability of hosting guest molecules [143] and sensing traces of toxic [19–21] or explosive compounds [24,144], ions [106,145], and in light-emitting diodes (LED) [13].

In 2018, one such functional coordination polymer was published by Fromm at al. [26] using the 9,10-di(1H-imidazol-1-yl)anthracene ligand **80** in coordination with Zn[II] and Cd[II]. Due to the possible conjugation of the nitrogen lone pair in the imidazole moiety, which leads to the partial formation of the double bond, the molecule is not completely flexible. Nevertheless, rotation is still possible but quite slow, allowing for of two conformers to form, cis and trans (Scheme 12).
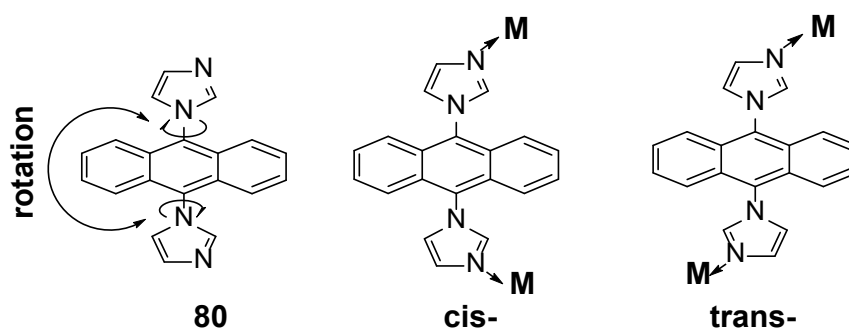
Scheme 12. Ligand L: 9,10-di(1-H-imidazol-1-yl)-anthracene and its cis- and trans-conformations in coordination polymers.

Interestingly even though the molar ratio of the ligand to the metal salt used in the reaction was always 1:1, the resulting coordination polymer featured a 2:1 ratio for ligand and metal. In addition, it has been found that by changing the polarity of the solvent mixture, the ligand L can adopt either the cis- (polar solvent, e.g., MeOH/DCM (1/4)) or the trans-conformation (e.g., MeOH/DCM (4/1)), whereas in an intermediate solvent mixture (e.g., MeOH/dioxane (1/4)), both forms are present. These possible modifications led to the synthesis of several different (1D, 2D, and 3D) coordination polymers (Figure 62), all showing a strong blue emission in the solid state at room temperature (Figure 63).

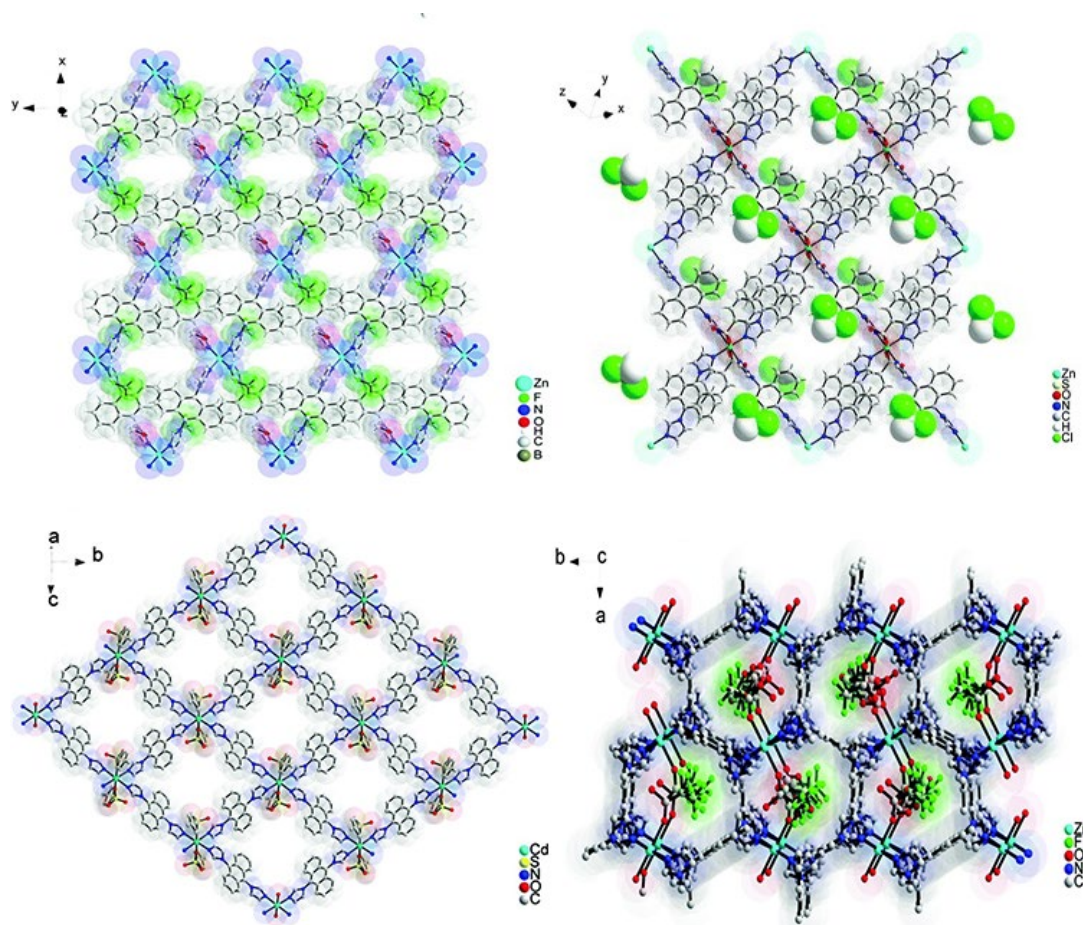**Figure 62.** Different structures obtained using ligand **80** in different solvents DCM/MeOH/CHCl₃. Adapted with permission from Ref. [26]. Copyright 2019, Royal Society of Chemistry.
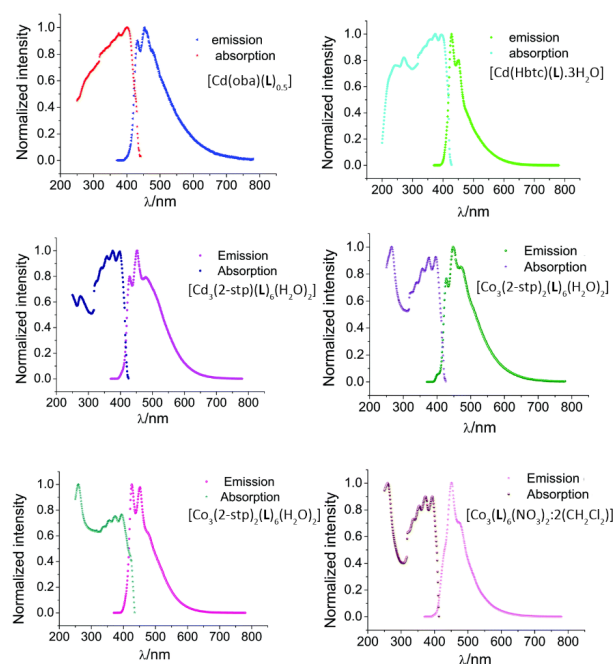

Figure 63. Solid-state UV–VIS and photoluminescence spectra of coordination polymer base of compounds **80** measured at 25 °C, excited at 350 nm. Adapted with permission from Ref. [26]. Copyright 2019, Royal Society of Chemistry.

In 2019, the same group published a different (1D and 2D) coordination polymer based on pyridyl-substituted anthracene building blocks **81**, simply by using different anions with either zinc or cadmium ions (Figure 64).

[Cd(oba)(**L**)$_{0.5}$]
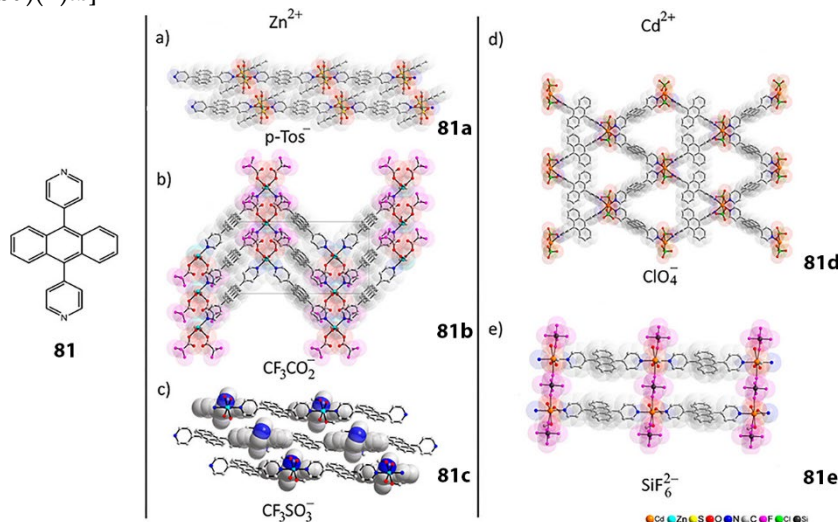
Figure 64. 1D (**a–c**) and 2D (**d,e**) coordination polymers obtained using ligand **81** with different metals (Zn^{II}, or Cd^{II}) and anions (*p*-Tos$^-$, CF$_3$CO$_2^-$, CF$_3$SO$_3^-$, ClO$_4^-$, SiF$_6^{2-}$). Adapted with permission from Ref. [23]. Copyright 2019, American Chemsitry Society.

The perchlorate (ClO$_4^-$) and hexafluoro silicon anion (SiF$_6^{2-}$) led to the formation of 2D structures, whereas tosylate (*p*-Tos$^-$), trifluoroacetate (CF$_3$CO$_2^-$), and triflate (CF$_3$SO$_3^-$) led to the formation of 1D coordination polymers. In both types, the ratio of ligand to metal was 2:1 (Figure 64). In addition, coordination polymer **88d** was capable of tracing different nitroaromatic and herbicide compounds down to ppb concentrations (Figure 65) [23].
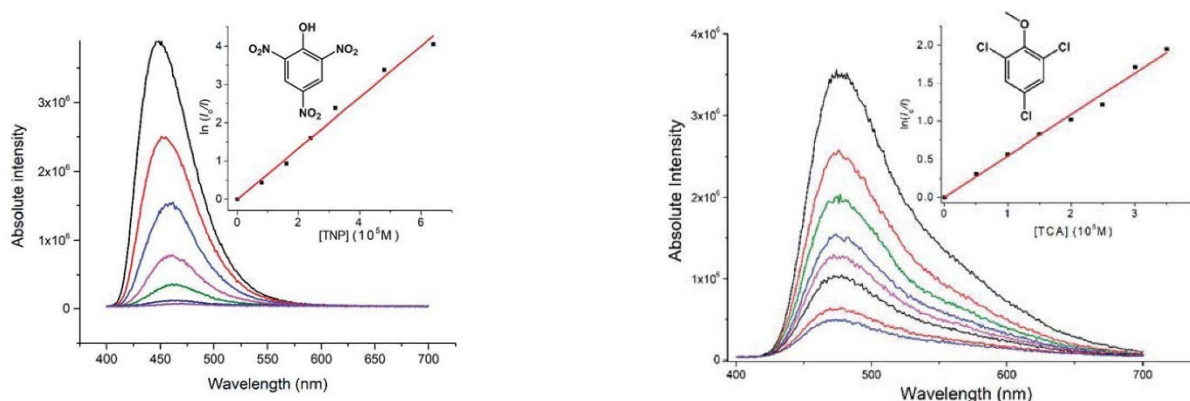
Figure 65. Fluorescence sensing of picric acid (TNP) (**left**) and 2,4,6-trichloroanisole (TCA) (**right**) by **88d** in MeCN. Adapted with permission from Ref. [23]. Copyright 2019, American Chemsitry Society.

The high sensing capability of such compounds for the above-mentioned nitro and herbicide compounds was possible due to the fluorescent emission of the compounds, which diminished in the presence of small quantities of the guest molecules. However, the mechanism on how the fluorescence emission is quenched is not well understood, but it is well known that these compounds are quite sensitive to the environment.

However, changing the ratio of the ligand to metal ion can also lead to different structures. For instance, in 2009, by using a 1:1 ratio of compound **81** ligand-to-metal ions, Khlobystov et al. synthesized 1D coordination polymer (Figure 66) [141].
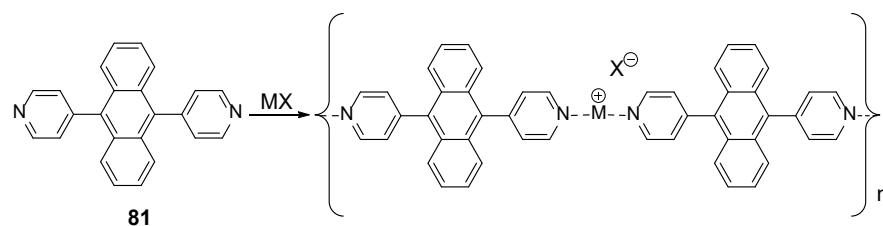
Figure 66. 1D coordination polymer of **81** in the presence of the metal (M = Ag^I, Zn^{II}, Cd^{II}, or Hg^{II}) in 1:1 ratio M = Ag^I, Zn^{II}, Cd^{II}, or Hg^{II}; X = NO$_3^-$, CF$_3$COO$^-$, CH$_3$COO$^-$, Cl$^-$, BF$_4^-$, ClO$_4^-$. Adapted with permission from Ref. [141]. Copyright 2009, WILEY-VCH Verlag GmbH & Co. KGaA.

One year later, in 2010, Fromm et al. [106] synthesized nanowire upon the reaction of **82** with silver metal ions. The resulting CP with a zigzag 1D chain due to the coordination of nitrogen atom from the pyridyl group to the silver ion displayed excimer emission owing to the pairwise stacking of anthracene moieties (Figure 67).

Hey-Hawkins et al. [146] confirmed that anthracene-based ligands are excellent candidates for the formation of CPs by using them for the detection of hydrogen peroxide (H$_2$O$_2$). Usually, anthracene-based ligands are used thanks to their excellent luminescent properties, which, in combination with sophisticated fluorimetry techniques, allow the detection of different analytes at very low concentrations.

The detection of singlet oxygen (^{1}O$_2$) based on an anthracene coordination polymer is also reported [147]. The author took advantage of the flexible anthracene ligand **83** (Figure 68, left) to synthesis a one-dimensional zigzag coordination polymer (Figure 68, right).
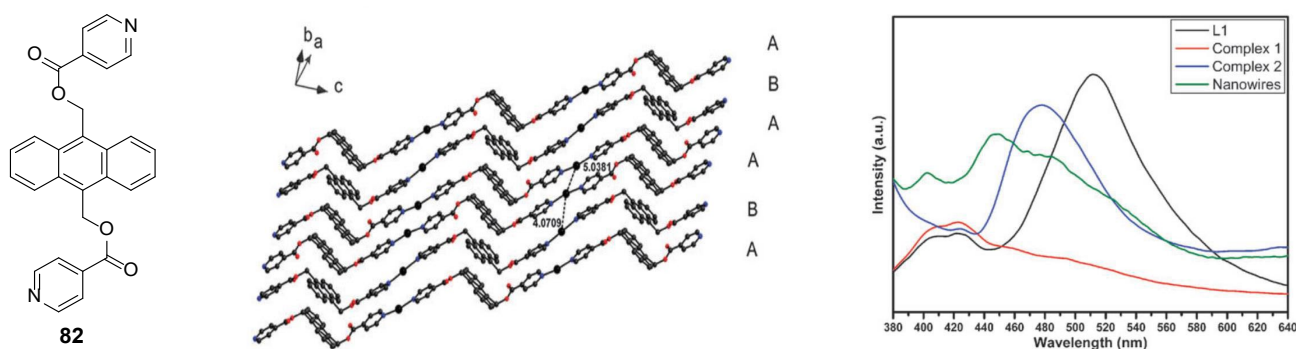
Figure 67. Chemical structure of L-82 (**left**), packing of the coordination polymer chains (**center**) and emission spectra of 82 and complexe (**right**), (excitation wave length is 344 nm). Adapted with permission from Ref. [107]. Copyright 2013, The Royal Society of Chemistry.
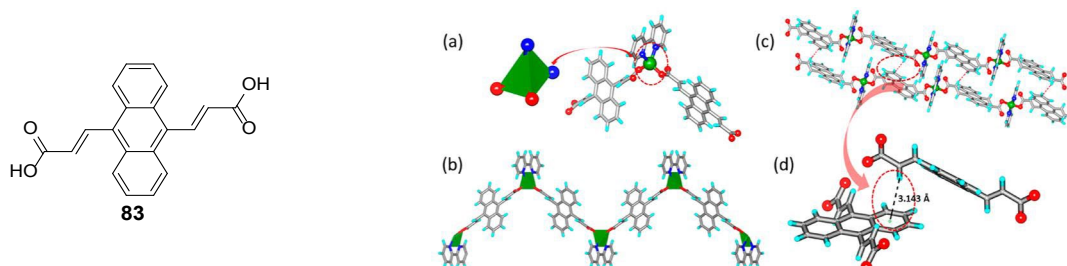
Figure 68. Chemical structure of 3,3′-(anthracene-9,10-diyl) diacrylic acid **84** and its coordination environment around the Zn(II) ions (**a–d**). Color codes: Zn, green; N, blue; C, gray; H, cyan; O, red. [147]. Adapted with permission from Ref. [147]. Copyright 2017, American Chemistry Society.

Ligand **84** showed aggregation-induced emission (AIE) activity in ethanol/hexane medium. However, in the crystal structure of the CP, the same ligand adopted a different (twisted diacrylic) conformation. This change in the structure of ligand **83** led to a drastic change in the photophysical properties of CP (λ_{max} = 500 nm), in comparison with the ligand alone (λ_{max} = 580 nm) with a hypsochromic shift of 80 nm (Figure 69). The origin of this type of emission is attributed to the twisted diacrylic ligand conformation compared with the free ligand and to the rigidity in the resulting CP.
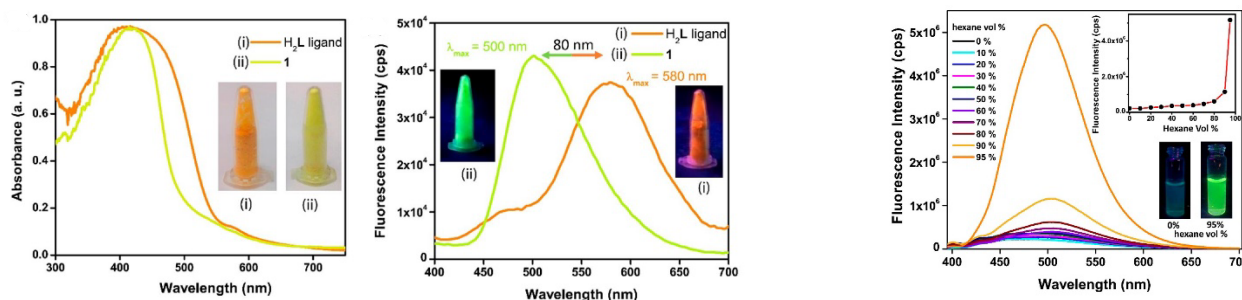
Figure 69. (**Left**) Solid-state absorption and (**middle**) emission spectra of Cp and **83** ligand at room temperature. (**Right**) Change in the fluorescence emission spectra of **83** ligand (50 μM) with a change of hexane vol% in ethanol. Adapted with permission from Ref. [147]. Copyright 2017, American Chemistry Society.

In addition to it, the resulting coordination polymer showed an expressed fluorescence response toward singlet oxygen ($^1O_2$) in a very selective manner (Figure 70) [148–150]. The mechanism of sensing, on the other hand, is also well known [58,64,151,152], as the singlet oxygen reacts with anthracene building in a [4 + 2] cycloaddition, leading to the formation of endoperoxides, which, due to the subsequent loss of aromaticity (conjugation), have low or no fluorescence at all.
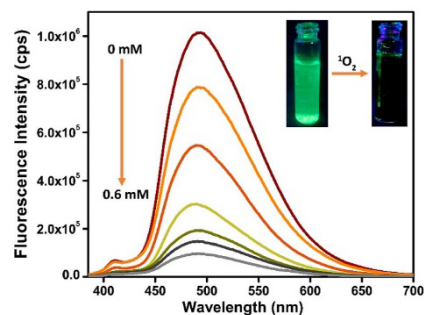
**Figure 70.** Change in the fluorescence emission intensity of **83** with an increasing concentration of $^1O_2$ solution. Inset: corresponding fluorescent images under a UV lamp. Adapted with permission from Ref. [147]. Copyright 2017, American Chemistry Society.

Besides simple coordination systems based on a single ligand, one can also use additional auxiliary ligands (e.g., **L-84** (1,4-H₂bdc) and **L-85** (2,6-H₂ndc)) for the construction of coordination polymers (Figure 71).
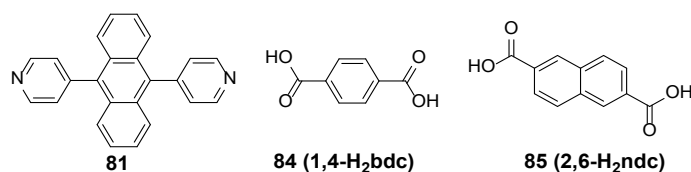
Figure 71. Chemical structure ligands.

Thus, the solvothermal reaction of **81** in tandem with **84** gives the compound **86** or in tandem with **85** gives the compound **87**, or **88** in the presence of either Zn(II) or Cd(II) salt led to the synthesis of three different 3D coordination polymers (Figure 72) [153].
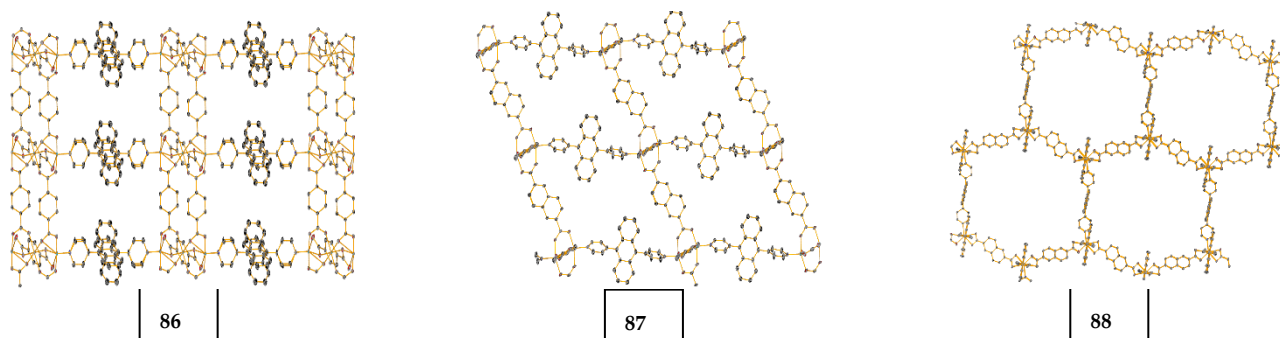
Figure 72. Three-dimensional architecture of **86**, **87**, and **88**. Adapted with permission from Ref. [153]. Copyright 2017, Elsevier B.V.

These CPs in Figure 72 display strong luminescence emissions, which are stronger than the one of ligand **81** alone due to high-dimensional structures of the CPs and the rigidity enhancement of the ligand, thus minimizing the loss of energy through radiationless pathways (Figure 73). Therefore, such compounds have the potential to be used in photoelectronic devices, such as LEDs.
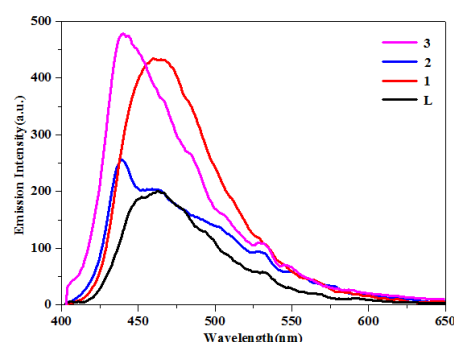
Figure 73. The solid-state emission spectra of **81** and complexes at room temperature.

2. Conclusions

In summary, we have given an introduction about the photophysical properties of organic compounds with special emphasis on that of anthracene and its derivatives, as well as the interaction of light with matter, explaining in detail the Jablonski diagram. In addition, we have provided the reader with a brief introduction of the importance of the fluorescence/fluorimetry technique as a highly sensitive method for tracing toxic and explosive compounds, as well as for bioimaging in biology and medicine. Furthermore, different types of aggregates formed in both the ground and the excited state and their influence on the outcome of the emission light are discussed, and intermolecular energy/electron transfer in dyads and triads is briefly covered to give the readers a bit of a flavor of such compounds.

Author Contributions: A.K. and K.M.F. drew the plan for this review. A.K. and F.O. contributed equally to the drafting of the manuscript. A.S. and K.M.F. revised and corrected the manuscript. All authors have read and agreed to the published version of the manuscript.

Conflicts of Interest: The authors declare no conflict of interest.

References

1. Kumar, N. *Comprehensive Physics for Class XII*; Laxmi Publications: New Delhi, India, 2004.
2. Tanaka, A.; Makino, A. Photosynthetic research in plant science. *Plant Cell Physiol.* **2009**, *50*, 681–683.
3. Ciamician, G. The Photochemistry of the Future. *Science* **1912**, *36*, 385–394.
4. Bayrakçeken, F. Triplet–triplet optical energy transfer from benzophenone to naphthalene in the vapor phase. *Spectrochim. Acta Part A Mol. Biomol. Spectrosc.* **2008**, *71*, 603–608.
5. Contributors, P.L. UV-Visible Spectral Features of Benzine and Some PAHs. Available online: https://publiclab.org/notes/warren/8-5-2011/uv-visible-spectral-features-benzine-and-some-pahs (accessed on 9 September 2020).
6. Jones, R.N. The Ultraviolet Absorption Spectra of Anthracene Derivatives. *Chem. Rev.* **1947**, *41*, 353–371.
7. Lucy, W.; Pickett, L.W.; Muntz, M.; McPherson, E.M. Vacuum Ultraviolet Absorption Spectra of Cyclic Compounds. I. Cyclohexane, Cyclohexene, Cyclopentane, Cyclopentene and Benzene1. *J. Am. Chem. Soc.* **1951**, *73*, 4862–4865.
8. National Institute of Standards and Technology. Cyclohexane. Available online: https://webbook.nist.gov/cgi/cbook.cgi?ID=C110827&Mask=400#UV-Vis-Spec (accessed on 10 September 2020).
9. Paris, J.P.; Brandt, W.W. Charge Transfer Luminescence of A Ruthenium(II) Chelate. *J. Am. Chem. Soc.* **1959**, *81*, 5001–5002.
10. Laporte, O.; Meggers, W.F. Some Rules of Spectral Structure*. *J. Opt. Soc. Am.* **1925**, *11*, 459–463.
11. Wardle, B. *Principles and Applications of Photochemistry*; John Wiley: Chichester, UK, 2009.
12. Lavis, L.D.; Raines, R.T. Bright Ideas for Chemical Biology. *ACS Chem. Biol.* **2008**, *3*, 142–155.
13. Xu, H.; Chen, R.; Sun, Q.; Lai, W.; Su, Q.; Huang, W.; Liu, X. Recent progress in metal–organic complexes for optoelectronic applications. *Chem. Soc. Rev.* **2014**, *43*, 3259–3302.
14. Huang, J.; Su, J.-H.; Tian, H. The development of anthracene derivatives for organic light-emitting diodes. *J. Mater. Chem.* **2012**, *22*, 10977–10989.
15. Sun, C.-Y.; Wang, X.-L.; Zhang, X.; Qin, C.; Li, P.; Su, Z.-M.; Zhu, D.-X.; Shan, G.-G.; Shao, K.-Z.; Wu, H.; et al. Efficient and tunable white-light emission of metal–organic frameworks by iridium-complex encapsulation. *Nat. Commun.* **2013**, *4*, 2717.
16. Gupta, A. Aggregation-Induced Emission: A Tool for Sensitive Detection of Amines. *ChemistrySelect* **2019**, *4*, 12848–12860.
17. Jung, H.S.; Kwon, P.S.; Lee, J.W.; Kim, J.I.; Hong, C.S.; Kim, J.W.; Yan, S.; Lee, J.Y.; Lee, J.H.; Joo, T.; et al. Coumarin-Derived Cu2+-Selective Fluorescence Sensor: Synthesis, Mechanisms, and Applications in Living Cells. *J. Am. Chem. Soc.* **2009**, *131*, 2008–2012.
18. Rosenthal, J.; Lippard, S.J. Direct Detection of Nitroxyl in Aqueous Solution Using a Tripodal Copper(II) BODIPY Complex. *J. Am. Chem. Soc.* **2010**, *132*, 5536–5537.
19. Montalti, M.; Prodi, L.; Zaccheroni, N. Luminescent Chemosensors Based on Anthracene or Dioxyxanthone Derivatives. *J. Fluoresc.* **2000**, *10*, 71.
20. Räupke, A.; Palma-Cando, A.; Shkura, E.; Teckhausen, P.; Polywka, A.; Görrn, P.; Scherf, U.; Riedl, T. Highly sensitive gas-phase explosive detection by luminescent microporous polymer networks. *Sci. Rep.* **2016**, *6*, 29118.
21. Gu, T.-Y.; Dai, M.; Young, D.J.; Ren, Z.-G.; Lang, J.-P. Luminescent Zn(II) Coordination Polymers for Highly Selective Sensing of Cr(III) and Cr(VI) in Water. *Inorg. Chem.* **2017**, *56*, 4668–4678.
22. Haldar, R.; Prasad, K.; Samanta, P.K.; Pati, S.; Maji, T.K. Luminescent Metal–Organic Complexes of Pyrene or Anthracene Chromophores: Energy Transfer Assisted Amplified Exciplex Emission and Al3+ Sensing. *Cryst. Growth Des.* **2016**, *16*, 82–91.
23. Vasylevskyi, S.I.; Bassani, D.M.; Fromm, K.M. Anion-Induced Structural Diversity of Zn and Cd Coordination Polymers Based on Bis-9,10-(pyridine-4-yl)-anthracene, Their Luminescent Properties, and Highly Efficient Sensing of Nitro Derivatives and Herbicides. *Inorg. Chem.* **2019**, *58*, 5646–5653.
24. Gong, W.-J.; Ren, Z.-G.; Li, H.-X.; Zhang, J.-G.; Lang, J.-P. Cadmium(II) Coordination Polymers of 4-Pyr-poly-2-ene and Carboxylates: Construction, Structure, and Photochemical Double [2 + 2] Cycloaddition and Luminescent Sensing of Nitroaromatics and Mercury(II) Ions. *Cryst. Growth Des.* **2017**, *17*, 870–881.
25. Shaligram, S.; Wadgaonkar, P.P.; Kharul, U.K. Fluorescent polymeric ionic liquids for the detection of nitroaromatic explosives. *J. Mater. Chem. A* **2014**, *2*, 13983–13989.
26. Vasylevskyi, S.I.; Regeta, K.; Ruggi, A.; Petoud, S.; Piguet, C.; Fromm, K.M. cis- and trans-9,10-di(1H-imidazol-1-yl)-anthracene based coordination polymers of ZnII and CdII: Synthesis, crystal structures and luminescence properties. *Dalt Trans.* **2018**, *47*, 596–607.
27. Shanmugaraju, S.; Mukherjee, P.S. π-Electron rich small molecule sensors for the recognition of nitroaromatics. *Chem. Commun.* **2015**, *51*, 16014–16032.
28. Shanmugaraju, S.; Mukherjee, P.S. Self-Assembled Discrete Molecules for Sensing Nitroaromatics. *Chem. Eur. J.* **2015**, *21*, 6656–6666.
29. Nagarkar, S.S.; Joarder, B.; Chaudhari, A.K.; Mukherjee, S.; Ghosh, S.K. Highly Selective Detection of Nitro Explosives by a Luminescent Metal–Organic Framework. *Angew. Chem. Int. Ed.* **2013**, *52*, 2881–2885.
30. Tsien, R.Y. Constructing and Exploiting the Fluorescent Protein Paintbox (Nobel Lecture). *Angew. Chem. Int. Ed.* **2009**, *48*, 5612–5626.
31. Stepanenko, O.V.; Stepanenko, O.V.; Shcherbakova, D.M.; Kuznetsova, I.M.; Turoverov, K.K.; Verkhusha, V.V. Modern fluorescent proteins: From chromophore formation to novel intracellular applications. *BioTechniques* **2011**, *51*, 313–327.
32. Drobizhev, M.; Makarov, N.S.; Tillo, S.E.; Hughes, T.E.; Rebane, A. Two-photon absorption properties of fluorescent proteins. *Nat. Methods* **2011**, *8*, 393–399.
33. Goedhart, J.; van Weeren, L.; Hink, M.A.; Vischer, N.O.E.; Jalink, K.; Gadella, T.W.J. Bright cyan fluorescent protein variants identified by fluorescence lifetime screening. *Nat. Methods* **2010**, *7*, 137–139.
34. Zimmer, M. GFP: From jellyfish to the Nobel prize and beyond. *Chem. Soc. Rev.* **2009**, *38*, 2823–2832.

35. Rae, M.; Fedorov, A.; Berberan-Santos, M.N. Fluorescence quenching with exponential distance dependence: Application to the external heavy-atom effect. *J. Chem. Phys.* **2003**, *119*, 2223–2231.

36. Najbar, J.; Mac, M. Mechanisms of fluorescence quenching of aromatic molecules by potassium iodide and potassium bromide in methanol–ethanol solutions. *J. Chem. Soc. Faraday Trans.* **1991**, *87*, 1523–1529.

37. Probst, B.; Guttentag, M.; Rodenberg, A.; Hamm, P.; Alberto, R. Photocatalytic H2 Production from Water with Rhenium and Cobalt Complexes. *Inorg. Chem.* **2011**, *50*, 3404–3412.

38. Förster, T. *Fluorescence of Organic Compounds*; Vandenhoeck und Ruprecht: Gottingen, Germany, 1951; p. 312.

39. Chamorro-Garcia, A.; Merkoçi, A. Nanobiosensors in diagnostics. *Nanobiomedicine* **2016**, *3*, 1849543516663574.

40. Srivastava, R.; Kamalasanan, M.N.; Chauhan, G.; Kumar, A.; Tyagi, P.; Kumar, A. Organic Light Emitting Diodes for White Light Emission. In *Organic Light Emitting Diode*; Mazzeo, M., Ed.; InTech: London, UK, 2010; ISBN 978-953-307-140-4.

41. Dexter, D.L. A Theory of Sensitized Luminescence in Solids. *J. Chem. Phys.* **1953**, *21*, 836–850.

42. Rehm, D.; Weller, A. Kinetik und Mechanismus der Elektronübertragung bei der Fluoreszenzlöschung in Acetonitril. Zeitschrift für Elektrochemie, Berichte der Bunsengesellschaft für physikalische Chemie (Zeitschrift für Elektrochemie, Berichte der Bunsengesellschaft für physikalische Chemie). *Ber. Bunsenges. Phys. Chem.* **1969**, *73*, 834–839.

43. Watkins, A.R. Short-lived intermediates formed by the interaction between electronically excited molecules and inorganic ions. *J. Phys. Chem.* **1974**, *78*, 1885–1890.

44. Rhodes, A.A.; Swartz, B.L.; Hosler, E.R.; Snyder, D.L.; Benitez, K.M.; Chohan, B.S.; Basu, S. Static quenching of tryptophan fluorescence in proteins by a dioxomolybdenum(VI) thiolate complex. *J. Photochem. Photobiol. A* **2014**, *293*, 81–87.

45. Mehra, J.; Rechenberg, H. *The Fundamental Equations of Quantum Mechanics, 1925–1926*, 1st softcover print; Springer: New York, NY, USA, 2001; ISBN 0387951784.

46. Franz, K.A.; Kehr, W.G.; Siggel, A.; Wieczoreck, J.; Adam, W. *Luminescent materials, In Ullmann's Encyclopedia of Industrial Chemistry*; Ullmann, F., Ed.; Wiley: Weinheim, Germany, 2002; pp. 591–627.

47. Clabau, F.; Rocquefelte, X.; Jobic, S.; Deniard, P.; Whangbo, M.-H.; Garcia, A.; Le Mercier, T. Mechanism of Phosphorescence Appropriate for the Long-Lasting Phosphors Eu2+-Doped SrAl2O4 with Codopants Dy3+ and B3+. *Chem. Mater.* **2005**, *17*, 3904–3912.

48. Zitoun, D.; Bernaud, L.; Manteghetti, A.; Filhol, J.-S. Microwave Synthesis of a Long-Lasting Phosphor. *J. Chem. Educ.* **2009**, *86*, 72.

49. Rocke, A.J. It Began with a Daydream: The 150th Anniversary of the Kekulé Benzene Structure. *Angew. Chem. Int. Ed.* **2015**, *54*, 46–50.

50. Yeh-Yung Lin, R.; Lin, H.-W.; Yen, Y.-S.; Chang, C.-H.; Chou, H.-H.; Chen, P.-W.; Hsu, C.-Y.; Chen, Y.-C.; Lin, J.T.; Ho, K.-C. 2,6-Conjugated anthracene sensitizers for high-performance dye-sensitized solar cells. *Energy Environ. Sci.* **2013**, *6*, 2477–2486.

51. Teng, C.; Yang, X.; Yang, C.; Li, S.; Cheng, M.; Hagfeldt, A.; Sun, L. Molecular Design of Anthracene-Bridged Metal-Free Organic Dyes for Efficient Dye-Sensitized Solar Cells. *J. Phys. Chem. C* **2010**, *114*, 9101–9110.

52. Cho, I.; Kim, S.H.; Kim, J.H.; Park, S.; Park, S.Y. Highly efficient and stable deep-blue emitting anthracene-derived molecular glass for versatile types of non-doped OLED applications. *J. Mater. Chem.* **2012**, *22*, 123–129.

53. Uchimura, M.; Watanabe, Y.; Araoka, F.; Watanabe, J.; Takezoe, H.; Konishi, G. Development of Laser Dyes to Realize Low Threshold in Dye-Doped Cholesteric Liquid Crystal Lasers. *Adv. Mater.* **2010**, *22*, 4473–4478.

54. Kanamaru, N. Radiationless Transition between Randomly Fluctuating Levels. S1-T2-T1 Intersystem Crossing in Condensed Phase. *Bull. Chem. Soc. Jpn.* **1982**, *55*, 3093–3096.

55. Yildiz, A.; Reilley, C.N. The Mechanism of Intersystem Crossing for Some Substituted Aromatic Hydrocarbons. *Spectrosc. Lett* **1968**, *1*, 335–343.

56. Coudret, C.; Mazenc, V. Heteroarylation of anthraquinone-triflate by suzuki cross-coupling. *Tetrahedron Lett.* **1997**, *38*, 5293–5296.

57. Zhao, J.; Chen, K.; Hou, Y.; Che, Y.; Liu, L.; Jia, D. Recent progress in heavy atom-free organic compounds showing unexpected intersystem crossing (ISC) ability. *Org. Biomol. Chem.* **2018**, *16*, 3692–3701.

58. Musgrave, C.O. Oxidation of alkyl aryl ethers. *Chem. Rev.* **1968**, *69*, 499–531.

59. Heilbron , M.I.; Heaton, S.J. 9,10-DIBROMOANTHRACENE. *Org. Synth.* **1923**, *3*, 41.

60. Jacob, J.; Espenson, J.H. Selective C-H bond activation of arenes catalyzed by methylrhenium trioxide. *Inorg. Chim. Acta* **1998**, *270*, 55–59.

61. Marshall, J.L.; Lehnherr, D.; Lindner, B.D.; Tykwinski, R.R. Reductive Aromatization/Dearomatization and Elimination Reactions to Access Conjugated Polycyclic Hydrocarbons, Heteroacenes, and Cumulenes. *ChemPlusChem* **2017**, *82*, 967–1001.

62. Bachmann, W.E.; Chemerda, J.M. The Synthesis of 9,10-Dimethyl-1,2-benzanthracene, 9,10-Diethyl-1,2-benzanthracene and 5,9,10-Trimethyl-1,2-benzanthracene. *J. Am. Chem. Soc.* **1938**, *60*, 1023–1026.

63. Martinez, G.R.; Ravanat, J.-L.; Medeiros, M.H.G.; Cadet, J.; Di Mascio, P. Synthesis of a Naphthalene Endoperoxide as a Source of 18O-labeled Singlet Oxygen for Mechanistic Studies. *J. Am. Chem. Soc.* **2000**, *122*, 10212–10213.

64. Fudickar, W.; Linker, T. Synthesis of Pyridylanthracenes and Their Reversible Reaction with Singlet Oxygen to Endoperoxides. *J. Org. Chem.* **2017**, *82*, 9258–9262.

65. Fritzsche, J.J. Ueber die festen Kohlenwasserstoffe des Steinkohlentheers. *Prakt. Chem.* **1867**, *101*, 333.

66. Breton, G.W.; Vang, X. Photodimerization of Anthracene. *J. Chem. Educ.* **1998**, *75*, 81.

67. Greene, F.D.; Misrock, S.L.; Wolfe, J.R. The Structure of Anthracene Photodimers. *J. Am. Chem. Soc.* **1955**, *77*, 3852–3855.

68. Bhatnagar, S.S.; Kapur, P.L.; Kaur, G. Photopolymerisation of anthracene in benzene solution from the magnetic standpoint. *Proc. Indian Acad. Sci.* **1939**, *10*, 468.

69. Bouas-Laurent, H.; Castellan, A.; Desvergne, J.-P.; Lapouyade, R. Photodimerization of anthracenes in fluid solutions: (Part 2) Mechanistic aspects of the photocycloaddition and of the photochemical and thermal cleavage. *Chem. Soc. Rev.* **2001**, *30*, 248–263.

70. Becker, H.D. Unimolecular photochemistry of anthracenes. *Chem. Rev.* **1993**, *93*, 145–172.

71. Julian, M.M. Mechanism of photodimerization in single crystals of anthracene. *Acta Cryst.* **1973**, *29*, 116–120.

72. Kusukawa, T.; Kojima, Y.; Kannen, F. Mechanofluorochromic Properties of 1,8-Diphenylanthracene Derivatives. *Chem. Lett.* **2019**, *48*, 1213–1216.

73. Luo, X.; Li, J.; Li, C.; Heng, L.; Dong, Y.Q.; Liu, Z.; Bo, Z.; Tang, B.Z. Reversible Switching of the Emission of Diphenyldibenzofulvenes by Thermal and Mechanical Stimuli. *Adv. Mater.* **2011**, *23*, 3261–3265.

74. Xue, P.; Yang, Z.; Chen, P. Hiding and revealing information using the mechanochromic system of a 2,5-dicarbazole-substituted terephthalate derivative. *J. Mater. Chem. C* **2018**, *6*, 4994–5000.

75. Zelzer, M.; Kappaun, S.; Zojer, E.; Slugovc, C. Synthesis and Photo Physical Properties of 9,10-Bis(hydroxyphenyl)anthracene Derivatives. *Monatsh. Chem.* **2007**, *138*, 453–464.

76. Zhang, W.; Wang, Q.; Feng, X.; Yang, L.; Wu, Y.; Wei, X. Anthracene-based derivatives: Synthesis, photophysical properties and electrochemical properties. *Chem. Res. Chin. Univ.* **2017**, *33*, 603–610.

77. Hu, J.-Y.; Feng, X.; Seto, N.; Do, J.-H.; Zeng, X.; Tao, Z.; Yamato, T. Synthesis, structural and spectral properties of diarylamino-functionalized pyrene derivatives via Buchwald–Hartwig amination reaction. *J. Mol. Struct.* **2013**, *1035*, 19–26.

78. Xiaorong Wang; Sanxiao Zhao; Yin Chen; Jingang Wang. Synthesis and photophysical properties of multilayer emitting π-p-π fluorophores. *Spectrochim. Acta A* **2020**, *227*, 117680.

79. Fan, Y.; Zhao, Y.; Ye, L.; Li, B.; Yang, G.; Wang, Y. Polymorphs and Pseudopolymorphs of N , N -Di(n -butyl)Quinacridone: Structures and Solid-State Luminescence Properties. *Cryst. Growth Des.* **2009**, *9*, 1421–1430.

80. Kohmoto, S.; Tsuyuki, R.; Masu, H.; Azumaya, I.; Kishikawa, K. Polymorphism-dependent fluorescence of 9,10-bis(pentafluorobenzoyloxy)anthracene. *Tetrahedron Lett.* **2008**, *49*, 39–43.

81. Zhang, Z.; Zhang, Y.; Yao, D.; Bi, H.; Javed, I.; Fan, Y.; Zhang, H.; Wang, Y. Anthracene-Arrangement-Dependent Emissions of Crystals of 9-Anthrylpyrazole Derivatives. *Cryst. Growth Des.* **2009**, *9*, 5069–5076.

82. Venkataramana, G.; Sankararaman, S. Synthesis and Spectroscopic Investigation of Aggregation through Cooperative π–π and C–H···O Interactions in a Novel Pyrene Octaaldehyde Derivative. *Org. Lett.* **2006**, *8*, 2739–2742.

83. Curtis, M.D.; Cao, J.; Kampf, J.W. Solid-State Packing of Conjugated Oligomers: From π-Stacks to the Herringbone Structure. *J. Am. Chem. Soc.* **2004**, *126*, 4318–4328.

84. Dong, J.; Solntsev, K.M.; Tolbert, L.M. Activation and Tuning of Green Fluorescent Protein Chromophore Emission by Alkyl Substituent-Mediated Crystal Packing. *J. Am. Chem. Soc.* **2009**, *131*, 662–670.

85. An, B.-K.; Kwon, S.-K.; Jung, S.-D.; Park, S.Y. Enhanced Emission and Its Switching in Fluorescent Organic Nanoparticles. *J. Am. Chem. Soc.* **2002**, *124*, 14410–14415.

86. Bricks, J.L.; Slominskii, Y.L.; Panas, I.D.; Demchenko, A.P. Fluorescent J-aggregates of cyanine dyes: Basic research and applications review. *Methods Appl. Fluoresc.* **2017**, *6*, 12001.

87. Xiao, J.; Yin, Z.; Yang, B.; Liu, Y.; Ji, L.; Guo, J.; Huang, L.; Liu, X.; Yan, Q.; Zhang, H.; et al. Preparation, characterization, physical properties, and photoconducting behaviour of anthracene derivative nanowires. *Nanoscale* **2011**, *3*, 4720–4723.

88. Hoeben, F.J.; Jonkheijm, P.; Meijer, E.W.; Schenning, A.P. About Supramolecular Assemblies of π-Conjugated Systems. *Chem. Rev.* **2005**, *105*, 1491–1546.

89. Ajayaghosh, A.; Praveen, V.K. π-Organogels of Self-Assembled p-Phenylenevinylenes: Soft Materials with Distinct Size, Shape, and Functions. *Acc. Chem. Res.* **2007**, *40*, 644–656.

90. Grimsdale, A.C.; Müllen, K. The Chemistry of Organic Nanomaterials. *Angew. Chem. Int. Ed.* **2005**, *44*, 5592–5629.

91. Kim, S.; Fujitsuka, M.; Tohnai, N.; Tachikawa, T.; Hisaki, I.; Miyata, M.; Majima, T. The unprecedented J-aggregate formation of rhodamine moieties induced by 9-phenylanthracenyl substitution. *Chem. Commun.* **2015**, *51*, 11580–11583.

92. Sekiguchi, K.; Yamaguchi, S.; Tahara, T. Formation and Dissociation of Rhodamine 800 Dimers in Water: Steady-State and Ultrafast Spectroscopic Study. *J. Phys. Chem. A* **2006**, *110*, 2601–2606.

93. Xue, S.; Qiu, X.; Sun, Q.; Yang, W. Alkyl length effects on solid-state fluorescence and mechanochromic behavior of small organic luminophores. *J. Mater. Chem. C* **2016**, *4*, 1568–1578.

94. Chan, J.M.W.; Tischler, J.R.; Kooi, S.E.; Bulović, V.; Swager, T.M. Synthesis of J-Aggregating Dibenz[a,j]anthracene-Based Macrocycles. *J. Am. Chem. Soc.* **2009**, *131*, 5659–5666.

95. Banerjee, S.; Both, A.K.; Sarkar, M. Probing the Aggregation and Signaling Behavior of Some Twisted 9,9'-Bianthryl Derivatives: Observation of Aggregation-Induced Blue-Shifted Emission. *ACS Omega* **2018**, *3*, 15709–15724.

96. Gruszecki, W.I. Structural characterization of the aggregated forms of violaxanthin. *J. Biol. Phys.* **1991**, *18*, 99–109.

97. Gierschner, J.; Ehni, M.; Egelhaaf, H.-J.; Milián Medina, B.; Beljonne, D.; Benmansour, H.; Bazan, G.C. Solid-state optical properties of linear polyconjugated molecules: π-stack contra herringbone. *J. Chem. Phys.* **2005**, *123*, 144914.

98. Gierschner, J.; Lüer, L.; Milián-Medina, B.; Oelkrug, D.; Egelhaaf, H.-J. Highly Emissive H-Aggregates or Aggregation-Induced Emission Quenching? The Photophysics of All-Trans para-Distyrylbenzene. *J. Phys. Chem. Lett.* **2013**, *4*, 2686–2697.

99. Wang, H.; Li, F.; Gao, B.; Xie, Z.; Liu, S.; Wang, C.; Hu, D.; Shen, F.; Xu, Y.; Shang, H.; et al. Doped Organic Crystals with High Efficiency, Color-Tunable Emission toward Laser Application. *Cryst. Growth Des.* **2009**, *9*, 4945–4950.

100. Wu, D.-E.; Wang, M.-N.; Luo, Y.-H.; Zhang, Y.-W.; Ma, Y.-H.; Sun, B.-W. Tuning the structures and photophysical properties of 9,10-distyrylanthrance (DSA) via fluorine substitution. *New J. Chem.* **2017**, *41*, 4220–4233.

101. Ferguson, J. Absorption spectroscopy of sandwich dimers and cyclophanes. *Chem. Rev.* **1986**, *86*, 957–982.

102. Vollbrecht, J. Excimers in organic electronics. *New J. Chem.* **2018**, *42*, 11249–11254.

103. Dey, S.; Mondal, P.; Rath, S.P. Aggregation-controlled excimer emission in an axial anthracene–Sn(iv)porphyrin–anthracene triad in the solid and solution phases. *New J. Chem.* **2015**, *39*, 4100–4108.

104. Wannasiri, C.; Chanmungkalakul, S.; Bunchuay, T.; Chuenchom, L.; Uraisin, K.; Ervithayasuporn, V.; Kiatkamjornwong, S. Cross-Linking Silsesquioxane Cages with Polyaromatics as Fluorescent Porous Polymers for Fluoride Sensing and Removal. *ACS Appl. Polym. Mater.* **2020**, *2*, 1244–1255.

105. Birks, J.B. Excimers. *Rep. Prog. Phys.* **1975**, *38*, 903–974.

106. Chen, J.; Neels, A.; Fromm, K.M. Excimer formation in crystalline and nanostructured coordination polymers. *Chem. Commun.* **2010**, *46*, 8282–8284.

107. Yamane, S.; Sagara, Y.; Kato, T. Steric effects on excimer formation for photoluminescent smectic liquid-crystalline materials. *Chem. Commun.* **2013**, *49*, 3839–3841.

108. Hinoue, T.; Shigenoi, Y.; Sugino, M.; Mizobe, Y.; Hisaki, I.; Miyata, M.; Tohnai, N. Regulation of π-Stacked Anthracene Arrangement for Fluorescence Modulation of Organic Solid from Monomer to Excited Oligomer Emission. *Chem. Eur. J.* **2012**, *18*, 4634–4643.

109. Gao, Y.; Liu, H.; Zhang, S.; Gu, Q.; Shen, Y.; Ge, Y.; Yang, B. Excimer formation and evolution of excited state properties in discrete dimeric stacking of an anthracene derivative: A computational investigation. *Phys. Chem. Chem. Phys.* **2018**, *20*, 12129–12137.

110. Liu, H.; Yao, L.; Li, B.; Chen, X.; Gao, Y.; Zhang, S.; Li, W.; Lu, P.; Yang, B.; Ma, Y. Excimer-induced high-efficiency fluorescence due to pairwise anthracene stacking in a crystal with long lifetime. *Chem. Commun.* **2016**, *52*, 7356–7359.

111. Jaseer, M.; Prasad, E. Room temperature anthracene excimer emission from self-assembled (aminomethyl)anthracene derivatives in plastic crystalline phase. *J. Photochem. Photobiol. A* **2010**, *214*, 248–256.

112. Luo, D.; Liao, C.-W.; Chang, C.-H.; Tsai, C.-C.; Lu, C.-W.; Chuang, T.C.; Chang, H.-H. Approach to Fast Screen the Formation of an Exciplex. *J. Phys. Chem. C* **2020**, *124*, 10175–10184. https://doi.org/10.1021/acs.jpcc.0c00825.

113. Huang, F.; Feng, G. Highly selective and controllable pyrophosphate induced anthracene-excimer formation in water. *RSC Adv.* **2014**, *4*, 484–487.

114. Ban, X.; Sun, K.; Sun, Y.; Huang, B.; Jiang, W. Enhanced Electron Affinity and Exciton Confinement in Exciplex-Type Host: Power Efficient Solution-Processed Blue Phosphorescent OLEDs with Low Turn-on Voltage. *ACS Appl. Mater. Interfaces* **2016**, *8*, 2010–2016.

115. Kim, J.-M.; Lee, C.-H.; Kim, J.-J. Mobility balance in the light-emitting layer governs the polaron accumulation and operational stability of organic light-emitting diodes. *Appl. Phys. Lett.* **2017**, *111*, 203301.

116. Zhang, Y.; Mali, B.L.; Geddes, C.D. Metal-enhanced fluorescence exciplex emission. *Spectrochim. Acta Part A Mol. Biomol. Spectrosc.* **2012**, *85*, 134–138.

117. Chen, L.-Y.; Shiu, Y.-J.; Wu, Y.-J.; Huang, W.-Y. Simple structured color tunable white organic light-emitting diodes utilizing an ambipolar anthracene derivative with low-lying LUMO. *Org. Electron.* **2020**, *76*, 105454.

118. Bowen, E.J. Fluorescence quenching in solution and in the vapour state. *Trans. Faraday Soc.* **1954**, *50*, 97–102.

119. Labianca, D.A.; Taylor, G.N.; Hammond, G.S. Structure-reactivity factors in the quenching of fluorescence from naphthalenes by conjugated dienes. *J. Am. Chem. Soc.* **1972**, *94*, 3679–3683.

120. Weller, A. Electron-transfer and complex formation in the excited state. *Pure Appl. Chem.* **1968**, *16*, 115–124.

121. Ohshiro, I.; Ikegami, M.; Nishimura, Y.; Arai, T. Exciplex Formation of Intermolecularly Hydrogen-Bonded System between Anthracene and N,N-Dimethylaniline Derivatives. *Bull. Chem. Soc. Jpn.* **2006**, *79*, 1950–1954.

122. Yang, N.C.; Shold, D.M.; Kim, B. Chemistry of exciplexes. 5. Photochemistry of anthracene in the presence and absence of dimethylaniline. *J. Am. Chem. Soc.* **1976**, *98*, 6587–6596.

123. Yang, N.C.; Shold, D.M.; McVey, J.K. Chemistry of exciplexes. III. Exciplex fluorescence from anthracene and substituted anthracenes in the presence of 2,5-dimethyl-2,4-hexadiene. *J. Am. Chem. Soc.* **1975**, *97*, 5004–5005.

124. Kazuhiko Mizuno/Chyongjin Pac/Hiroshi Sakurai. Photochemical reactions of aromatic compounds. XIX. Photocycloaddition of olefins to 9-cyanophenanthrene. Singlet exciplex or triplet mechanism depending on olefins. *J. Am. Chem. Soc.* **1974**, *96*, 2993–2994.

125. Cann, J.R.; Cabanetos, C.; Welch, G.C. Synthesis of Molecular Dyads and Triads Based Upon N-Annulated Perylene Diimide Monomers and Dimers. *Eur. J. Org. Chem.* **2018**, *2018*, 6933–6943.

126. Bureš, F. Fundamental aspects of property tuning in push–pull molecules. *RSC Adv.* **2014**, *4*, 58826–58851.

127. Brunner, K.; Van Dijken, A.; Börner, H.; Bastiaansen, J.J.; Kiggen, N.M.; Langeveld, B.M. Carbazole Compounds as Host Materials for Triplet Emitters in Organic Light-Emitting Diodes: Tuning the HOMO Level without Influencing the Triplet Energy in Small Molecules. *J. Am. Chem. Soc.* **2004**, *126*, 6035–6042.

128. Matteucci, E.; Baschieri, A.; Sambri, L.; Monti, F.; Pavoni, E.; Bandini, E.; Armaroli, N. Carbazole-Terpyridine Donor-Acceptor Dyads with Rigid π-Conjugated Bridges. *ChemPlusChem* **2019**, *84*, 1353–1365.

129. Ge, J.-Z.; Zou, Y.; Yan, Y.-H.; Lin, S.; Zhao, X.-F.; Cao, Q.-Y. A new ferrocene–anthracene dyad for dual-signaling sensing of Cu(II) and Hg(II). *J. Photochem. Photobiol. A Chem.* **2016**, *315*, 67–75.

130. Hauschild, M.; Chen, L.; Etschel, S.H.; Ferguson, M.J.; Hampel, F.; Halik, M.; Tykwinski, R.R. Anthracene-Pentacene Dyads: Synthesis and OFET Characterization. *ChemPlusChem* **2020**, *85*, 921–926.

131. Etschel, S.H.; Waterloo, A.R.; Margraf, J.T.; Amin, A.Y.; Hampel, F.; Jäger, C.M.; Clark, T.; Halik, M.; Tykwinski, R.R. An unsymmetrical pentacene derivative with ambipolar behavior in organic thin-film transistors. *Chem. Commun. (Camb. Engl.)* **2013**, *49*, 6725–6727.

132. Chaari, M.; Kelemen, Z.; Choquesillo-Lazarte, D.; Gaztelumendi, N.; Teixidor, F.; Viñas, C.; Nogués, C.; Núñez, R. Efficient blue light emitting materials based on m-carborane–anthracene dyads. Structure, photophysics and bioimaging studies. *Biomater. Sci.* **2019**, *7*, 5324–5337.

133. Chaari, M.; Kelemen, Z.; Planas, J.G.; Teixidor, F.; Choquesillo-Lazarte, D.; Ben Salah, A.; Viñas, C.; Núñez, R. Photoluminescence in m -carborane–anthracene triads: A combined experimental and computational study. *J. Mater. Chem. C* **2018**, *6*, 11336–11347.

134. Mahmood, Z.; Taddei, M.; Rehmat, N.; Bussotti, L.; Doria, S.; Guan, Q.; Ji, S.; Zhao, J.; Di Donato, M.; Huo, Y.; et al. Color-Tunable Delayed Fluorescence and Efficient Spin–Orbit Charge Transfer Intersystem Crossing in Compact Carbazole-Anthracene-Bodipy Triads Employing the Sequential Electron Transfer Approach. *J. Phys. Chem. C* **2020**, *124*, 5944–5957.

135. Sayfutyarova, E.R.; Hammes-Schiffer, S. Substituent Effects on Photochemistry of Anthracene–Phenol–Pyridine Triads Revealed bCd((y Multireference Calculations. *J. Am. Chem. Soc.* **2020**, *142*, 487–494.

136. Turro, N.J.; Ramamurthy, V.; Scaiano, J.C. *Modern molecular Photochemistry of Organic Molecules*; University Science Books: Sausalito, CA, USA, 2010.

137. Parada, G.A.; Goldsmith, Z.K.; Kolmar, S.; Pettersson Rimgard, B.; Mercado, B.Q.; Hammarström, L.; Hammes-Schiffer, S.; Mayer, J.M. Concerted proton-electron transfer reactions in the Marcus inverted region. *Science* **2019**, *364*, 471–475.

138. Ariga, K.; Hill, J.P.; Lee, M.V.; Vinu, A.; Charvet, R.; Acharya, S. Challenges and breakthroughs in recent research on self-assembly. *Sci. Technol. Adv. Mater.* **2008**, *9*, 14109.

139. Caulder, D.L.; Raymond, K.N. Supermolecules by Design. *Acc. Chem. Res.* **1999**, *32*, 975–982.

140. Batten, S.R.; Champness, N.R.; Chen, X.-M.; Garcia-Martinez, J.; Kitagawa, S.; Öhrström, L.; O'Keeffe, M.; Suh, M.P.; Reedijk, J. Coordination polymers, metal–organic frameworks and the need for terminology guidelines. *CrystEngComm* **2012**, *14*, 3001–3004.

141. Cui, X.; Khlobystov, A.N.; Chen, X.; Marsh, D.H.; Blake, A.J.; Lewis, W.; Champness, N.R.; Roberts, C.J.; Schröder, M. Dynamic Equilibria in Solvent-Mediated Anion, Cation and Ligand Exchange in Transition-Metal Coordination Polymers: Solid-State Transfer or Recrystallisation? *Chem. Euro J.* **2009**, *15*, 8861–8873.

142. Yaghi, O.M.; Li, G.; Li, H. Selective binding and removal of guests in a microporous metal–organic framework. *Nature* **1995**, *378*, 703–706.

143. Dalgarno, S.J.; Tucker, S.A.; Bassil, D.B.; Atwood, J.L. Fluorescent Guest Molecules Report Ordered Inner Phase of Host Capsules in Solution. *Science* **2005**, *309*, 2037–2039.

144. Wang, J.-H.; Li, G.-Y.; Liu, X.-J.; Feng, R.; Zhang, H.-J.; Zhang, S.-Y.; Zhang, Y.-H. A fluorescent anthracene-based metal–organic framework for highly selective detection of nitroanilines. *Inorg. Chim. Acta* **2018**, *473*, 70–74.

145. Wu, Z.-F.; Velasco, E.; Shan, C.; Tan, K.; Zhang, Z.-Z.; Hu, Q.; Xing, K.; Huang, X.; Li, J. Robust fluorescent calcium coordination polymers as Cu^{2+} sensors with high sensitivity and fast response. *J. Mater. Chem. C* **2020**, *8*, 6820–6825.

146. Aleksovska, A.; Lönnecke, P.; Hey-Hawkins, E. Zn- and Cd-based coordination polymers with a novel anthracene dicarboxylate ligand for highly selective detection of hydrogen peroxide. *Dalt Trans.* **2020**, *49*, 4817–4823.

147. Dalapati, R.; Nandi, S.; van Hecke, K.; Biswas, S. Fluorescence Modulation of an Aggregation-Induced Emission Active Ligand via Rigidification in a Coordination Polymer and Its Application in Singlet Oxygen Sensing. *Cryst. Growth Des.* **2019**, *19*, 6388–6397.

148. Pedersen, S.K.; Holmehave, J.; Blaikie, F.H.; Gollmer, A.; Breitenbach, T.; Jensen, H.H.; Ogilby, P.R. Aarhus sensor green: A fluorescent probe for singlet oxygen. *J. Org. Chem.* **2014**, *79*, 3079–3087.

149. Frausto, F.; Thomas, S.W. Ratiometric Singlet Oxygen Detection in Water Using Acene-Doped Conjugated Polymer Nanoparticles. *ACS Appl. Mater. Interfaces* **2017**, *9*, 15768–15775.

150. Kubát, P.; Henke, P.; Berzediová, V.; Štěpánek, M.; Lang, K.; Mosinger, J. Nanoparticles with Embedded Porphyrin Photosensitizers for Photooxidation Reactions and Continuous Oxygen Sensing. *ACS Appl. Mater. Interfaces* **2017**, *9*, 36229–36238.

151. Miyamoto, S.; Martinez, G.R.; Medeiros, M.H.G.; Di Mascio, P. Singlet molecular oxygen generated from lipid hydroperoxides by the russell mechanism: Studies using 18(O)-labeled linoleic acid hydroperoxide and monomol light emission measurements. *J. Am. Chem. Soc.* **2003**, *125*, 6172–6179.

152. Li, X.; Zhang, G.; Ma, H.; Zhang, D.; Li, J.; Zhu, D. 4,5-dimethylthio-4′-2-(9-anthryloxy)ethylthiotetrathiafulvalene, a highly selective and sensitive chemiluminescence probe for singlet oxygen. *J. Am. Chem. Soc.* **2004**, *126*, 11543–11548.

153. Dong, J.-L.; Wang, D.-Z.; Jia, Y.-Y.; Wang, D.-H. Three coordination polymers based on 9,10-di(pyridine-4-yl)anthracene ligand: Syntheses, structures and fluorescent properties. *J. Mol. Struct.* **2017**, *1142*, 304–310.